AMERICAN SOCIETY FOR MICROBIOLOGY | Journal of Virology®

VIRUS-CELL INTERACTIONS

Human Cytomegalovirus Utilizes Multiple Viral Proteins to Regulate the Basement Membrane Protein Nidogen 1

Man I Kuan,[a] Lisa B. Caruso,[b] Anamaria G. Zavala,[a] Pranav S. J. B. Rana,[a] John M. O'Dowd,[a] Italo Tempera,[b] Elizabeth A. Fortunato[a]

[a]Department of Biological Sciences and Center for Reproductive Biology, University of Idaho, Moscow, Idaho, USA
[b]The Wistar Institute, Philadelphia, Pennsylvania, USA

ABSTRACT Nidogen 1 (NID1) is an important basement membrane protein secreted by many cell types. We previously found that human cytomegalovirus (HCMV) infection rapidly induced chromosome 1 breaks and that the basement membrane protein NID1, encoded near the 1q42 break site, was downregulated. We have now determined that the specific breaks in and of themselves did not regulate NID1, rather interactions between several viral proteins and the cellular machinery and DNA regulated NID1. We screened a battery of viral proteins present by 24 hours postinfection (hpi) when regulation was induced, including components of the incoming virion and immediate early (IE) proteins. Adenovirus (Ad) delivery of the tegument proteins pp71 and UL35 and the IE protein IE1 influenced steady-state (ss) NID1 levels. IE1's mechanism of regulation was unclear, while UL35 influenced proteasomal regulation of ss NID1. Real-time quantitative PCR (RT-qPCR) experiments determined that pp71 downregulated *NID1* transcription. Surprisingly, WF28-71, a fibroblast clone that expresses minute quantities of pp71, suppressed *NID1* transcription as efficiently as HCMV infection, resulting in the near absence of ss NID1. Sequence analysis of the region surrounding the 1q42 break sites and *NID1* promoter revealed CCCTC-binding factor (CTCF) binding sites. Chromatin immunoprecipitation experiments determined that pp71 and CTCF were both bound at these two sites during HCMV infection. Expression of pp71 alone replicated this binding. Binding was observed as early as 1 hpi, and colocalization of pp71 and CTCF occurred as quickly as 15 min postinfection (pi) in infected cell nuclei. In fibroblasts where CTCF was knocked down, Adpp71 infection did not decrease *NID1* transcription nor ss NID1 protein levels. Our results emphasize another aspect of pp71 activity during infection and identify this viral protein as a key contributor to HCMV's efforts to eliminate NID1. Further, we show, for the first time, direct interaction between pp71 and the cellular genome.

IMPORTANCE We have found that human cytomegalovirus (HCMV) utilizes multiple viral proteins in multiple pathways to regulate a ubiquitous cellular basement membrane protein, nidogen-1 (NID1). The extent of the resources and the redundant methods that the virus has evolved to affect this control strongly suggest that its removal provides a life cycle advantage to HCMV. Our discoveries that one of the proteins that HCMV uses to control NID1, pp71, binds directly to the cellular DNA and can exert control when present in vanishingly small quantities may have broad implications in a wide range of infection scenarios. Dysregulation of NID1 in an immunocompetent host is not known to manifest complications during infection; however, in the naive immune system of a developing fetus, disruption of this developmentally critical protein could initiate catastrophic HCMV-induced birth defects.

KEYWORDS basement membrane, chromatin immunoprecipitation, human cytomegalovirus, protein-protein interactions, tegument

Editor Felicia Goodrum, University of Arizona

Address correspondence to Elizabeth A. Fortunato, lfort@uidaho.edu.

The authors declare no conflict of interest.

Received 29 August 2022
Accepted 6 September 2022
Published 11 October 2022

Human cytomegalovirus (HCMV) causes large changes in the mRNA and protein complement of infected host cells. In the past few years, the magnitude and range of these changes have been more thoroughly characterized with the advent of "big data" analyses (as reviewed in reference 1). Analyses of this type are effective at revealing wholesale changes to pathways affected by the presence of the virus, for instance, changes to innate antiviral response proteins, cell cycle and DNA repair proteins, proteins important to cellular differentiation and signaling, and developmentally important proteins. These analyses may open the door for more detailed examination of individual protein-protein interactions; however, they are sometimes overwhelming in scope, leaving it difficult to select single cellular proteins "worthy" of further analysis.

Our recent paper used the HCMV-induced site-specific break site at chromosome 1q42 as a springboard to focus our search for virus-regulated gene products (2, 3). Our analyses uncovered one gene adjacent to this locus, nidogen 1 (*NID1*), whose transcription was regulated by HCMV infection. Further analysis of NID1 protein stability also uncovered a proteasome-dependent regulation at the posttranslational level. We observed a decrease in both steady-state (ss) NID1 levels within the cell and the amount of protein secreted into the extracellular space beginning at approximately 24 hours postinfection (hpi) (3). Two large-scale transcriptomic/proteomic analyses confirmed the decreased transcription, ss protein levels, and secretion of NID1 we observed (4–6) (and M. Weekes, personal communication).

NID1 is an essential basement membrane (BM) protein that is involved in assembly, remodeling, and maintenance of BM integrity (7–9). NID1 acts as a bridge between collagen IV, the scaffold for all basement membranes, and laminin (7). These protein complexes bind to proteoglycans within the extracellular matrix (ECM), creating the support structure for developing organs. NID1 does not appear to be a "restriction factor" for HCMV; that is, removal of the protein from the cellular milieu did not increase efficiency of viral replication (3). We hypothesized that HCMV's efforts to reduce host NID1 may promote viral dissemination through the vasculature. Vascular wall BM integrity is maintained through secretion of NID1 by endothelial cells that line the vessels and by their underlying smooth muscle cells (SMCs) and fibroblasts (8–10). Downregulation of NID1 in infected endothelial cells may promote migration of monocytes through vessel walls, thereby increasing viral dissemination. In support of this hypothesis, we found increased monocyte transmigration through a confluent monolayer of NID1-knockdown (KD) cells (3).

Although there are numerous examples of HCMV-induced transcriptional and posttranslational changes to gene products, very few cellular proteins have been shown to be regulated in multiple ways by multiple viral proteins. BclAF1, which has been shown to be a restriction factor for HCMV, is targeted initially for proteasomal degradation by virion constituents pp71 and UL35 and then later in infection by the viral microRNA miR-UL112-1 (11). In the context of our study, work by Reinhardt and colleagues (12, 13) is also important. The authors found that collagen, a binding partner of NID1, was regulated at both the transcriptional and posttranslational levels in HCMV-infected smooth muscle cells; however, the viral proteins responsible were not determined. Large-scale data analyses have also identified several more cellular targets regulated by multiple mechanisms (4, 14) but have not defined the viral proteins responsible for most.

In this study, we sought to identify the viral constituents responsible for regulating NID1 and the pathways those players were acting upon. We also wanted to discern whether the HCMV-induced double-stranded DNA (dsDNA) breaks we have observed in every cell type with every viral strain and that occur within 15 min of exposure were causing a downregulation of NID1. CRISPR-mediated introduction of dsDNA breaks within a 1-kb region surrounding the mapped break sites did not downregulate ss NID1 protein levels. Using individual adenoviral (Ad) vector delivery, we found three viral proteins that regulated ss NID1 protein levels in the host cell, two tegument proteins, pp71 and UL35, and one IE protein, IE1. Although IE1 acted via an undefined mechanism to regulate this important BM protein, UL35, a known binding partner of

pp71 localized within the incoming virion tegument, showed a modest ability to regulate ss NID1 levels at the posttranslational level (as judged by proteasomal inhibition). Clear regulation of *NID1* mRNA production was observed after introduction of pp71. Astoundingly, the presence of an almost infinitesimal quantity of pp71 over an extended period was sufficient to reduce *NID1* transcription on par with infection. Here, we show that pp71 binds proximally to the 1q42 breaks and to the *NID1* promoter region of the cellular DNA. To the best of our knowledge, this is the first report of direct binding of pp71 to either viral or cellular DNA. Furthermore, we found that the CCCTC-binding factor (CTCF; the cellular insulator protein) is essential to pp71's *NID1* regulatory function and is also bound to these sites as early as 1 hpi. We believe our findings shed light on new regulatory roles for the viral proteins IE1, UL35, and pp71 and more firmly cement HCMV in the cadre of herpesviruses that coopt the regulatory mechanism of CTCF for their own ends.

RESULTS

Fine-mapping the HCMV-induced break site(s) at chromosome 1q42. Further investigation into the mechanism of the 1q42 break site required more precise mapping of its location. The mapped fluorescence *in situ* hybridization (FISH) clone G248P80968D1 (here after, 968 D1) bridging the 1q42 break site and its relationship to the *NID1* locus are shown in Fig. 1A; for reference, both the original NCBI genome annotation used to map the site (hg19) and the current annotation (hg38) are included. Finer mapping was performed using a methodology termed ligation-mediated PCR (LMPCR) (15) (see Materials and Methods for specifics). LMPCR is particularly useful when the approximate location of the double-stranded break (DSB) is known. Our earlier FISH mapping had defined an ~3.6-kb region within the bridging clone (968 D1) that lays between the proximal (G248P85799B5, hereafter B5) and distal (G248P87558G5, hereafter G5) fosmid clones. These clones overlapped 968 D1; however, FISH analysis demonstrated that they did not bridge the break site, suggesting that this ~3.6-kb region between B5 and G5 harbored the break site. DNA was extracted from mock- and virus-infected cells at 1 hpi and denatured. Biotinylated primers spanning the 3.6-kb region and approximately 500 bp into both flanking clones (B5 and G5) were hybridized. Primer extension reactions from two primers, 1q42-1F and 1q42-2F (marked in green in Fig. 1B), yielded blunt-ended fragments at the break sites of interest, allowing for linker ligation. These blunt-ended duplexes were then isolated on streptavidin beads, amplified with nested PCR, and sequenced to determine predominant DNA species in the virus-infected lanes (as described in detail in Materials and Methods). Comparison of those sequences to that of the 968 D1 clone sequence yielded four distinct break sites (Fig. 1B, lightning bolts).

CRISPR-induced generation of the HCMV-specific break sites revealed that neither breakage nor its repair were responsible for NID1 downregulation. CRISPR technology was used to replicate as closely as possible the HCMV-induced damage, with the goal of determining whether DSB induction, and its consequent inherently imperfect associated repair, regulated the ss NID1 level within the cell. Following available CRISPR design protocols (16), we synthesized six different guide RNAs (gRNAs) targeting the area surrounding the break sites (see Materials and Methods for specifics and sequences). The six gRNA sequences are outlined with red boxes in Fig. 1B. HEK 293T cells were used to grow individual lentiviruses, each designed to introduce one gRNA and Cas9 simultaneously. Human foreskin fibroblast (HFF) cells were transduced with one of the six lentiviruses, and pools of transduced cells were puromycin selected. To test the efficiency of break induction and repair within the pooled populations, cells were harvested, genomic DNA was extracted, and a 1-kb region surrounding the break site area was amplified (using primers 1q42-1N1 and 1q42-3R, see Materials and Methods). Using these two primers (and an additional primer [1q42-3F$_{int}$]) chosen to position the guide sequence roughly 200 to 400 bp from the start site, sequencing reactions were performed. We then used the tracking of indels by decomposition (TIDE) sequencing program (17) (https://tide.nki.nl/) to compare these CRISPR-generated

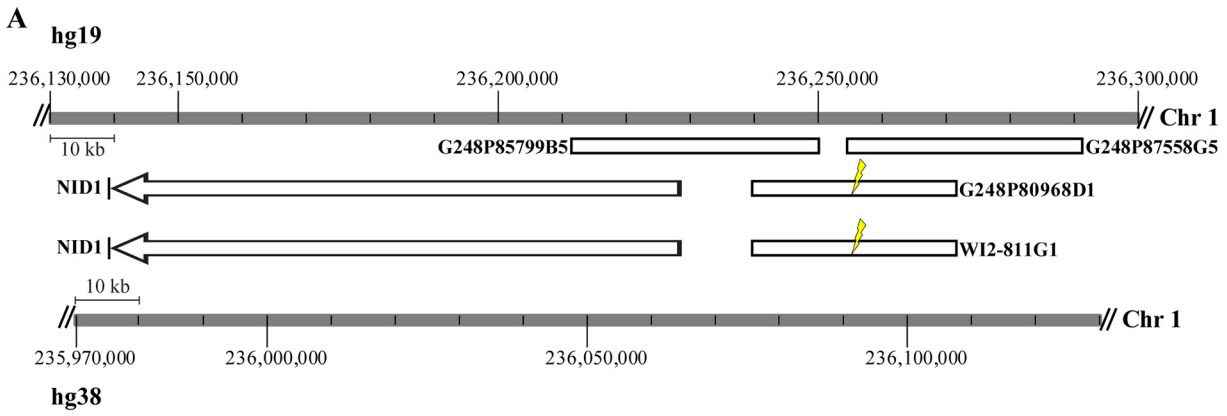

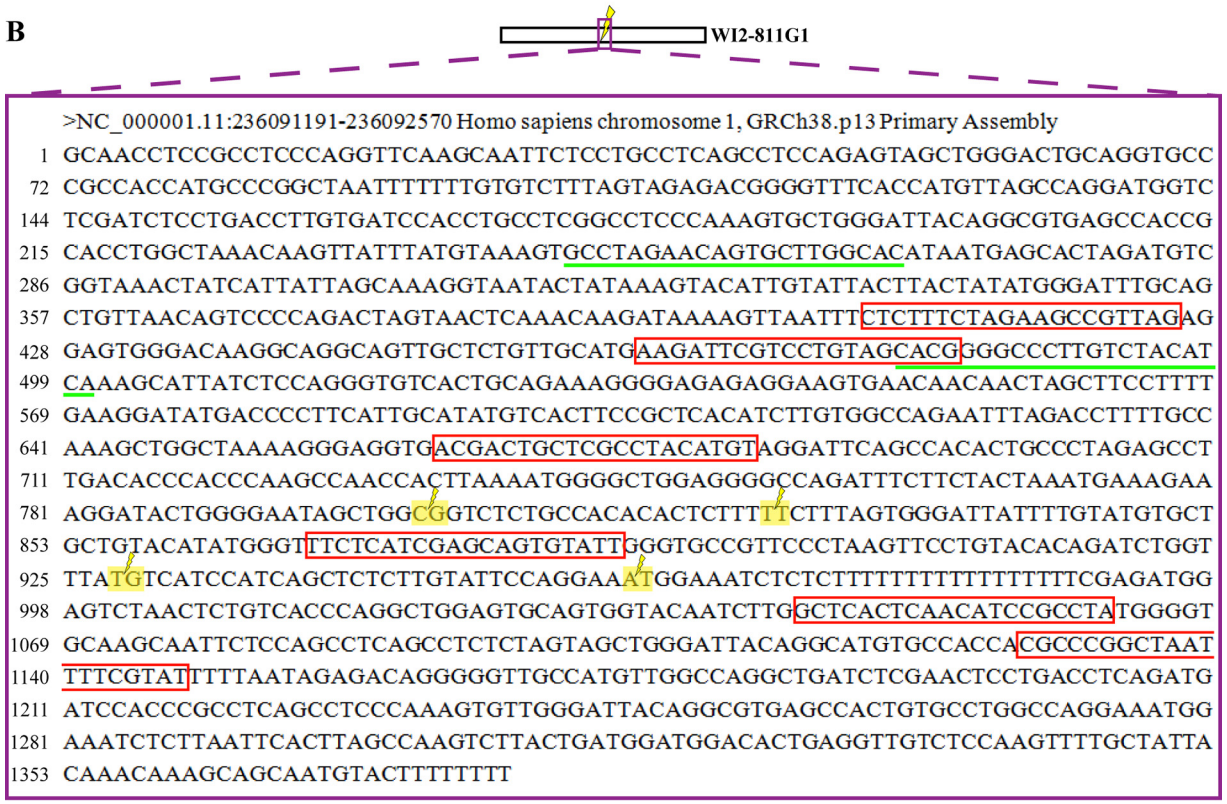

C

1q42 clone	Percentage (%) of break
v2.0	0
1	88
2	89
3	77
4	49
5	56
6	5

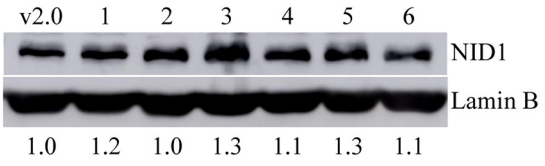

FIG 1 CRISPR-mediated breaks did not downregulate ss NID1 levels. (A) Diagram of locus surrounding the 1q42 break site in human genome versions hg19 and hg38. (B) Ligation-mediated PCR (LMPCR) identified four break sites (yellow highlight) on chromosome 1. Green underlined sequences indicate biotinylated primers used to identify these sites. The red boxes indicate the CRISPR gRNAs that were designed to target the area surrounding the mapped 1q42 breaks. (C) Table representing the percentage of CRISPR pooled populations with successful CRISPR-mediated breakage (and repair) targeting events in each of six 1q42 clones compared to control v2.0 pooled population using TIDE analysis. (D) The 1q42 clone 1 to 6 CRISPR pools (and v2.0 control pool) were seeded at equivalent densities and allowed to grow for 3 days before harvest. Cell lysates (25 μL) were assayed for NID1. Lamin B was used as a loading control. The number below each lane represents the intensity of the NID1 band normalized first to its loading control and then to the level of NID1 in the v2.0 control lane.

pool sequences to those generated by DNA amplification of control samples generated from cells with only the Cas9/gRNA backbone (v2.0) introduced. Fig. 1C shows a table representing the percentage of repaired breaks present within the given pooled populations. CRISPR targeting varied from essentially ineffective (5%, clone 6) to ~90% effective (clones 1 and 2). FISH had never detected infection-induced breaks above 30% of the infected population. Therefore, we considered these pools appropriate to assess if break induction (and repair) alone caused ss NID1 protein downregulation.

We seeded the clone 1 to 6 pooled populations and allowed them to grow for 3 days (alongside a control v2.0 population). Cells were then harvested and assayed for ss NID1 levels. Regardless of the break induction efficiency (5 to 90%), no change in the ss NID1 level was observed in these pooled cell populations (Fig. 1D). The number below each lane represents the intensity of the NID1 band normalized first to its loading control and then to the level of NID1 in the v2.0 control lane. It should be noted that these cells were passaged several times and resequenced to ensure that the "scars" of repair were still present. The TIDE comparisons and Western analyses were essentially identical after passaging. In fact, sequencing and protein analysis data represented in Fig. 1C and D are from the second round of analysis. Data from the first round of analysis of these clones are shown in Fig. S1A (TIDE) and S1B (Western blot) in the supplemental material. From these analyses, we concluded that break induction, and any potential nonfidelitous repair of those breaks, was not, at least solely, responsible for ss NID1 downregulation.

UV-inactivated virus downregulated ss NID1 levels. The absence of regulatory effects from the experiments described in Fig. 1 suggested that direct interactions between viral proteins and either the cellular DNA or its transcriptional/posttranslational machinery were responsible for ss NID1 downregulation. We had observed both transcriptional regulation and proteasomal degradation by 24 hpi (3). We reasoned that this implicated only viral proteins present by that time postinfection (pi). Prior to 24 hpi, the virus proteins present in HCMV-infected cells are limited to virion-delivered and rapidly synthesized viral proteins (i.e., the immediate early [IE] proteins).

UV-inactivated HCMV infections (+UV) were used to test the effect of the entire complement of virion-delivered proteins. As was previously shown (2, 18, 19), transit to the nucleus of nuclear localization signal (NLS)-encoding proteins (here exemplified by pp71 staining in red in Fig. 2A and B) was efficient in +UV infections. Virtually all cells, regardless of treatment of input virus, displayed pp71 staining at 4 hpi (rows 2 and 5 of Fig. 2A show higher magnifications, Fig. 2B shows a lower magnification, and Fig. 2C shows quantitation of pp71$^+$ cells). As expected, *de novo* expression of IE proteins (here exemplified by IE1 staining in green in Fig. 2A) was curtailed in +UV infections. Less than 4% of +UV-infected cells stained positive for IE1 at any time point analyzed (Fig. 2A and D), while the very large majority (~89%) of HCMV-infected cells were IE1$^+$ by 24 hpi (Fig. 2A and D). Note that while almost all +UV-infected cells were still pp71$^+$ at 24 hpi (Fig. 2C), the level of protein within the nucleus was substantially lower than in the HCMV-infected cells (compare rows 3 and 6 in Fig. 2A).

Samples of HCMV- and +UV-infected cells were analyzed for ss NID1 levels at 24 hpi via Western blotting (Fig. 2E). Lamin B was used as a loading control. As we had observed previously (3), ss NID1 levels in the HCMV-infected samples were markedly lower than in their mock-infected counterparts at this time point. Normalization of NID1 levels to levels of the loading control (see Materials and Methods for details) allowed for comparison of the levels of ss NID1 in the virus-treated to the mock-treated samples (V/M; see ratio below the blot in Fig. 2E). Somewhat surprisingly, the +UV-infected cells showed as robust a decrease in NID1 ss levels at this time point. This decrease in ss NID1 levels was observed in multiple different experiments, and the ratios of V/M for three different experiments are plotted in Fig. 2F. The difference in the observed intensity between infected and mock-infected samples reached statistical significance both with and without UV inactivation of HCMV.

We also analyzed *NID1* transcript levels at 24 hpi in HCMV- and +UV-infected

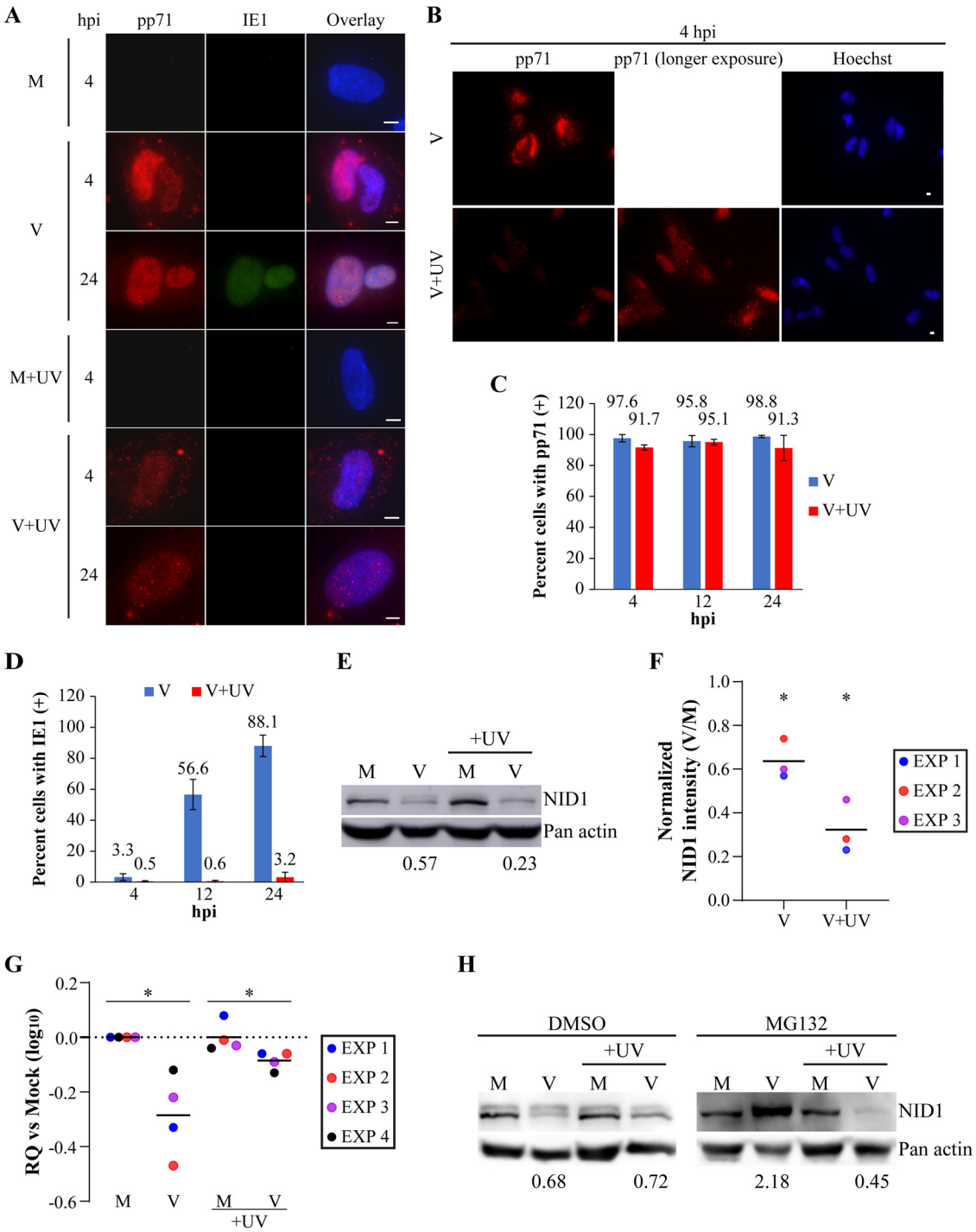

FIG 2 UV-inactivated virus downregulated ss NID1 levels. HFFs were infected with HCMV (V) or UV-inactivated (+UV) HCMV at an MOI of 5 and were harvested at the indicated time points pi. (A) Cells on coverslips were harvested at 4 and 24 hpi. Cells were stained for tegument protein pp71 (red) to assess input virions and IE1 (green) to assess *de novo* protein synthesis; scale bars, 5 μm in all figures; M, mock. (B) Whole fields of cells at 4 hpi are shown to indicate that essentially all cells are pp71$^+$ at this time point. A longer exposure (400 versus 200 ms) of +UV-infected cells is also shown for clarity. (C and D) Percent pp71$^+$ and IE1$^+$ cells at indicated time points pi, respectively. The mean of experiments was plotted. Error bars represent 1 standard error of the data. (E) Western blotting analysis of cell lysates (25 μL) for ss NID1 levels at 24 hpi with HCMV or +UV HCMV. Pan-actin was used as a loading control. Numbers below the blots represent normalized NID1 intensity of virus over mock samples (V/M) calculated for the given treatment (see Materials and Methods and text for details). (F) Scatter plot of three experiments for normalized NID1 (V/M) intensity as in Fig. 2E. Horizontal bars represent the mean of three experiments. Statistical analysis shows both HCMV and +UV infection caused statistically significant decreases in ss NID1 levels from mock-treated counterparts; Exp, experiment. (G) RT-qPCR analysis was performed to determine the levels of *NID1* transcripts at 24 hpi after HCMV or +UV infection. *G6PD* was used as the internal transcript control for normalization. Mock infection was used as the reference sample.

(Continued on next page)

samples in multiple experiments. As can be seen in Fig. 2G, a statistically significant decrease in transcript levels was observed in both infected populations. Note that since infected samples are compared to their mock-infected counterparts, a sample with a decreased level of transcripts would appear as a negative number on the graph. To address whether tegument-delivered proteins were involved in NID1 proteasomal degradation, we treated HCMV- or +UV-infected cells (along with their mock-infected counterparts) with either MG132 or a dimethyl sulfoxide (DMSO) vehicle control. Cells were harvested at 48 hpi to be consistent with our previous studies (3). As was expected given the results in Fig. 2E, the DMSO-treated HCMV- and +UV-infected samples showed decreased ss NID1 levels compared to their mock-infected counterparts (left side of Fig. 2H). Note that in this and multiple other blots throughout, we frequently observed NID1 running as a tight doublet in both the mock- and HCMV-infected lanes. We had observed this doublet in our previous studies (3) and discussed its potential significance there. As we had also observed previously, treatment with MG132 stabilized the ss NID1 level within the HCMV-infected cells (V lane in right side of Fig. 2H; note the increase in V/M ratio below the lane). NID1 stabilization was not observed in the +UV-infected cells. Possible reasons for this are discussed below. These experiments allowed us to conclude that viral input proteins were involved in the regulation of NID1.

At least two tegument proteins contributed to downregulation of ss NID1 levels. Having identified that virion-delivered components could regulate NID1, we focused attention on input tegument proteins in pursuit of a culpable member of that group. We individually expressed as many tegument proteins as possible to assess their impact on ss NID1 levels by using both adenovirus (Ad) and lentivirus delivery systems. Obvious candidates included the major tegument proteins pp65 and pp71, which have been shown to very rapidly transit to the nucleus after infection and influence antiviral activities of the cell (20, 21) (also as reviewed in reference 22). UL35, a known binding partner of pp71 and present in the virion, was an additional candidate for regulation of ss NID1. We also attempted to express the tegument proteins TRS1, IRS1, pp150, and UL69 via lentiviral transduction or plasmid expression followed by selection. Unfortunately, when expressed at high enough levels for long enough periods of time to assess their effect on ss NID1, all of these proteins proved toxic to the cells, preventing further analysis.

Ad delivery of pp65, pp71, and UL35 (see Materials and Methods for construction details) was robust, allowing us to vary multiplicity of infection (MOI)/level of protein delivery for our analyses. We first assessed the level of protein delivered to the cells at various MOIs compared to HCMV-infected cells (MOI of 5) harvested at 72 hpi. Expression of Adpp65, Adpp71, and AdUL35 produced equivalent or higher levels of their respective proteins than HCMV infection (Fig. 3A to C). As noted in the figure legend, lysate cell equivalents were adjusted in each of the blots so as not to overload the gels for the given protein of interest (leading to various levels of expression in the V lanes between Fig. 3A, B, and C, dependent on the amount of lysate loaded). Importantly, our AdUL35 construct (using a construct provided by Lori Frappier [23]) expressed not only full-length UL35 but also, as reported in the literature, low levels of UL35's C-terminal truncation UL35A (Fig. 3C), the functions of which may be quite distinct (23–25) (see Discussion for more information). During viral infection at 72 hpi, both proteins are expressed at relatively similar levels (see V lane in Fig. 3C). Our AdUL35 vector expressed a low level of UL35A compared to full-length UL35 (Fig. 3C, middle lanes show a longer exposure of the UL35A band region). To assess any contri-

FIG 2 Legend (Continued)
Four different experiments were performed, and the average value of triplicate samples from each experiment was plotted. Horizontal bars represent the mean of these four experiments; RQ, relative quantity. (H) At 4 hpi, 0.5 μM MG132 (or DMSO vehicle) was added to inhibit proteasomal activity. Cells were harvested at 48 hpi. Lysates (20 μL) were assayed for ss NID1 levels via Western blotting. Numbers below the blots represent normalized NID1 intensity for the given treatment (see Materials and Methods and text for details). Note DMSO and MG132 samples were run simultaneously but on different gels. Statistical significance between groups was as follows for all analyses reported: n.s., nonsignificant; n.s.$^{\Delta}$, P value between 0.05 and 0.08; *, $P < 0.05$; **, $P < 0.01$; ***, $P < 0.001$.

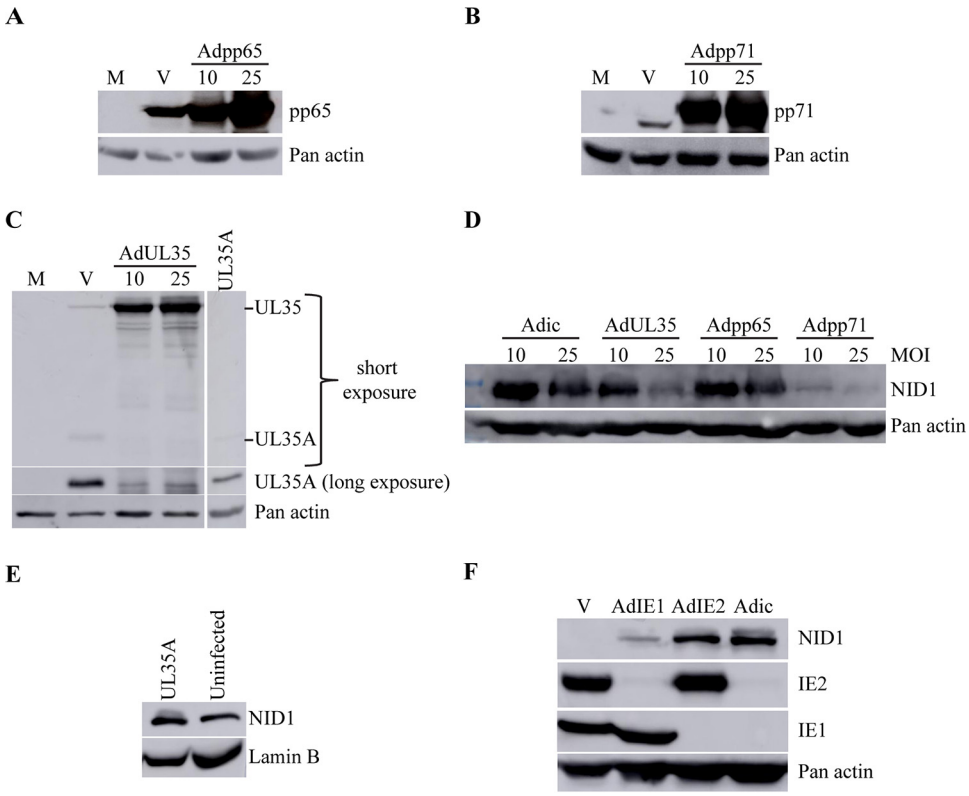

FIG 3 Tegument proteins pp71 and UL35 and immediate early protein IE1 downregulated ss NID1 levels. (A to C) HFFs were infected at the indicated MOI with Adpp65 (A), Adpp71 (B), or AdUL35 (C) or with HCMV at an MOI of 5 (V lane), harvested at 72 hpi, and assayed for the indicated tegument protein. Note that each blot used different lysate loading levels (A, 1 μL; B, 10 μL; C, 1 μL). The data in C also include cells infected with a UL35A-encoding retrovirus selected with puromycin, then reseeded and allowed to grow for 72 h. (D) HFFs infected with the indicated Ad vector at the indicated MOI were harvested at 72 hpi, and cell lysates (20 μL) were assayed for ss NID1. (E) UL35A retrovirus-infected HFFs were selected with puromycin, then reseeded and allowed to grow for 72 h. Cell lysates (20 μL) were assayed for ss NID1 levels. (F) HFFs were infected with Towne at an MOI of 5, AdIE1, AdIE2, or Adic (+Adtrans; all at an MOI of 10) and harvested at 72 hpi. Cell lysates (20 μL) were assayed via Western blotting for NID1, IE1 (monoclonal antibody p63-27), and IE2 (monoclonal antibody CH16.0). Pan-actin or lamin B was used as a loading control.

bution UL35A might have on its own, we obtained a retrovirus vector from Bonita Biegalke (24), encoding only the UL35A open reading frame. Infection with this construct followed by selection, seeding, and harvest after 72 h produced comparable levels of UL35A to those observed in the AdUL35 infections and similarly lower levels than those observed in HCMV-infected cells.

With these four constructs/vectors in hand, we infected HFFs and assessed the ss NID1 level at 72 hpi (Ad vectors, Fig. 3D compared to backbone Adic) or after selection and incubation for 72 hpi (retrovirus UL35A, Fig. 3E compared to uninfected cells). Ad infections were performed at MOIs of 10 and 25. Ad vectors delivered at an MOI of 50 were toxic to the cells over the extended time period needed for these analyses. Assessment of cell counts performed after MOI 25 experiments harvested at either 48 or 72 hpi showed no statistically significant differences between cells infected with Adpp65, AdUL35, Adpp71 or the backbone vector (Fig. S2). Neither Adpp65 (Fig. 3D) nor retroUL35A (Fig. 3E) affected ss NID1 levels at the input levels tested. Both AdUL35 and Adpp71 reduced the ss NID1 level, with Adpp71 exerting its effect at the lower MOI tested (Fig. 3D). Therefore, at least two tegument proteins, UL35 and pp71, delivered by HCMV regulated ss NID1 levels within the cell.

An HCMV IE protein also contributed to the downregulation of ss NID1 protein levels. Although we had observed virion-delivered protein involvement in ss NID1 downregulation, the timing (24 hpi) and well-documented role of several IE proteins in manipulating the cellular environment prompted us to also assess regulation of ss

NID1 by the two most abundant, and arguably most influential, IE proteins, IE1 and IE2. IE1 and IE2 were introduced using Ad delivery. Because relatively high levels of protein expression were necessary to assess their effects, and long-term expression of these proteins has been shown to be toxic to cells (26, 27), we utilized an inducible system developed by Dan Streblow. This system permits expression of high levels of the proteins only when an Ad vector-delivered transactivator is also present (see Materials and Methods and reference 27 for details). We first assessed the relative levels of each of the IE proteins expressed from our Ad vectors after induction with the transactivator in comparison to an HCMV infection (measured at 72 hpi because all other Ad infections were assessed at this time point). Ad expression of IE1 and IE2 proteins was comparable to that observed at 72 hpi in HCMV-infected cells (Fig. 3F). Infection with AdIE2 did not noticeably decrease ss NID1 compared to Adic; however, although not fully replicating HCMV infection-induced decreases, IE1 induced a substantial drop in ss NID1 levels in HFFs, adding an immediate early protein to the list of tegument proteins already uncovered.

UL35 promoted proteasomal degradation of NID1. Having previously determined that decreases in ss NID1 levels after infection were at least in part due to proteasomal degradation, we tested the three identified proteins for this ability (3). Fig. 4A demonstrates the degree of ss NID1 stabilization observed in HCMV-infected cells incubated beginning at 4 hpi with MG132, a proteasome inhibitor, and harvested at 48 hpi. We regularly observed a moderate decrease in ss NID1 in mock-treated samples after MG132 treatment, perhaps due to the relatively long incubation period; therefore, we adopted the same method of normalization described above (and in Materials and Methods) to compare the levels of protein in each lane. The values below each virus lane represent the value of the ratio of normalized V/M for the given treatment (DMSO versus MG132). The fold change observed in these ratios after treatment with MG132 is also indicated below the panel. In Fig. 4A, an increase in the V/M ratio of 8.3-fold, indicated that MG132 treatment led to a stabilization in the ss NID1 level and therefore an increase in V/M levels. Similar statistically significant differences were observed in multiple different experiments (Fig. 4B). Fig. 4C and D (Adpp65 and Adpp71), Fig. 4E and F (Adpp65 and AdUL35), and Fig. 4G and H (AdIE1) represent the data obtained after infecting cells at the indicated MOI (previously determined to affect ss NID1 levels) with a candidate protein (or with Adic as control) in the presence or absence of MG132. In Fig. 4C to F, MG132 was added at 4 hpi, with harvesting at 48 hpi as had been performed with HCMV infection. In Fig. 4G and H, cells were first allowed 24 h to express IE1 via transactivation and were then treated with MG132. Cells were harvested after an additional 48 h of incubation. Normalized Ad viral protein/Adic ratios obtained for each of the four viral proteins are shown below the appropriate treatment lanes for the representative experiments shown in Fig. 4C, E, and G. Data from additional experiments with statistical analysis of the observed differences are given in Fig. 4D, F, and H. Fig. 4C shows a less than 2-fold increase in this ratio in MG132-treated and Adpp71-infected cells. Although in multiple experiments, this increase never rose above 2-fold, it was statistically significant (Fig. 4D). In contrast, Fig. 4E shows that treatment with MG132 modestly increased the level of ss NID1 within the AdUL35-infected cells (by $\sim$ 4-fold). This modest increase was repeatedly observed, and the difference after treatment was statistically significant (Fig. 4F). Fig. 4G demonstrates that even when allowing an additional 24 h to express IE1 in the cells, the addition of MG132 provided no substantial stabilization of ss NID1 levels, with an increase that did not rise above 2-fold in multiple experiments and never reached statistical significance (Fig. 4H). Taken together, these results provided a first definitive, if not exclusive, identification of the viral protein UL35's involvement in proteasomal degradation of cellular NID1.

Infection with Adpp71 caused a substantial decrease in *NID1* mRNA transcripts. Having found a protein at least partly responsible for regulating ss NID1 protein levels, we next turned to an analysis of *NID1* transcription, which we had previously identified as being downregulated (3). We expressed Adpp71, AdUL35, and AdIE1 (and Adpp65 as a control) in cells to determine if one of them was responsible for the transcriptional downregulation after HCMV infection (shown in Fig. 5A for comparison). Note that all

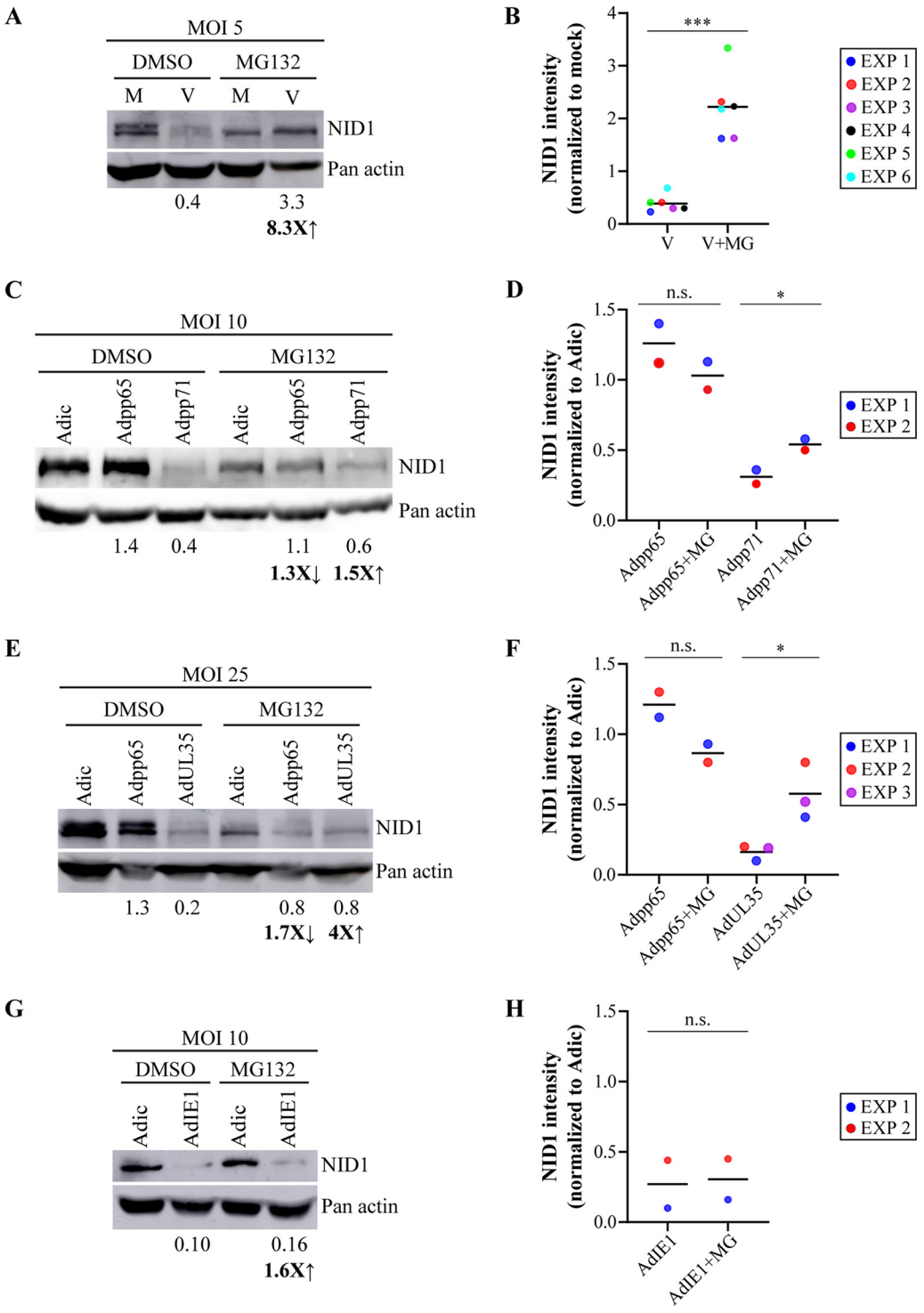

FIG 4 Tegument protein UL35 affected ss NID1 levels via the proteasome. HFFs were infected with HCMV (A) or the indicated Ad vector (C, E, and G) at the indicated MOI. At 4 hpi (A, C, and E) or 24 hpi (G), 0.5 μM MG132 (or DMSO vehicle) was added to inhibit proteasomal activity. Cells were harvested at 48 hpi (A, C, and E) or 72 hpi (G). Cell lysates (25 μL) were assayed via Western blotting for ss NID1. Pan-actin was used as a loading control to normalize the band intensity of NID1 for calculations of V/M or Ad viral protein/Adic ratios as described in Materials and Methods and the text and shown below each blot. (B, D, F, and H) Scatter plots of values of normalized NID1 intensity (V/M or Ad viral protein/Adic) ratios from different experiments like those represented in A, C, E, and G, respectively. Horizontal bars represent the means of repeated experiments.

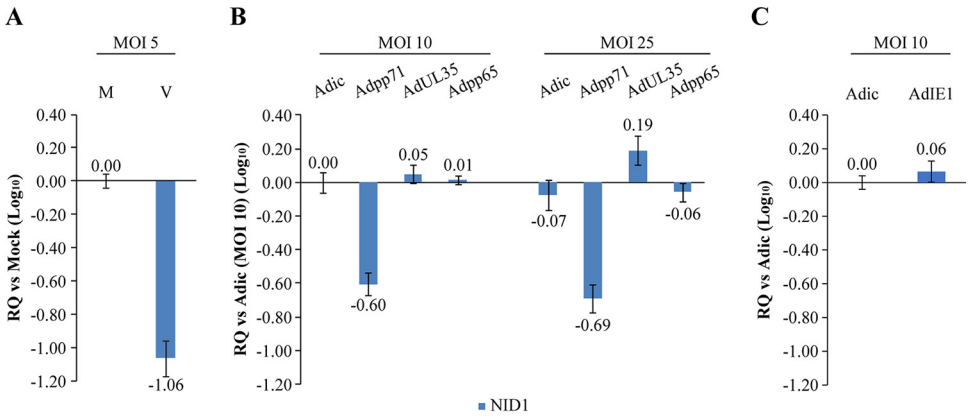

FIG 5 pp71 downregulated *NID1* transcription. HFFs were infected with Towne (A), Adpp71, AdUL35, or Adpp65 (B), or AdIE1 (+AdTrans) (C) or the indicated control (M or Adic) at the indicated MOI and harvested at 72 hpi. RT-qPCR analysis was performed to determine the level of *NID1* transcripts. *G6PD* was used as the internal transcript control for normalization. Data are presented as changes relative to mock-infected cells (A) or Adic-infected cells (B and C). See text for more detailed description.

panels represent mRNA extracted from cells harvested at 72 hpi. In each panel, the mock- or Adic-infected cells are used as the reference sample. Therefore, a sample with a decreased level of transcripts would appear as a negative number. For example, in Fig. 5A, HCMV-infected cells had a relative quantity of transcripts equivalent to -1.06 ($\log_{10}$) compared to mock-infected cells. This would be a decrease equivalent to ~10-fold. Expression of AdUL35 or Adpp65 at both MOIs tested exerted no effect on the level of transcripts; however, introduction of Adpp71 at the lower MOI of 10 induced marked downregulation (Fig. 5B). IE1 also did not influence the level of transcription from the *NID1* promoter (Fig. 5C). To this stage of investigation, our observations indicated that the degree of effect propagated by a single virus protein during short-term expression (72 h) never fully replicated that of an HCMV infection, reinforcing the synergistic and systemic nature of infection. Importantly, our experiments have not ruled out the potential for additional viral players in HCMV-induced NID1 regulation.

Sustained expression of an exceedingly small complement of pp71 downregulated ss NID1 levels. Sole expression of pp71 in HFFs regulated ss NID1; but, how much pp71 was necessary to exert these effects? We took advantage of a cell line previously described in the literature (WF28-71) (28), which was originally developed to complement the growth defects of a pp71-deficient virus. These cells express exceedingly low levels of pp71, as the expression of the protein is driven by a late viral promoter that is slightly "leaky." We observed the presence of very small foci/puncta of pp71 in the nuclei of these cells, reminiscent of those observed at both early and late times after +UV infection (compare Fig. 6A, bottom row to Fig. 2A). Cells infected with HCMV, harvested, and stained for pp71 at both 24 and 72 hpi are shown in Fig. 6A as a control for normal levels of pp71 observed within infected cells at these time points. Fig. 6B displays a relative quantitation of *pp71* transcript levels in the WF28-71 cells versus that observed after HCMV infection (at both 24 and 72 hpi). At these time points, the levels of *pp71* transcripts in infected cells were 1,700 and over 130,000 times more abundant than those measured in the WF28-71 cells, respectively.

Given the miniscule amount of transcripts observed in the WF28-71 cells, we were astounded that analysis of ss NID1 levels in these cells found decreases in protein comparable to those observed in HCMV-infected fibroblasts at 72 hpi (Fig. 6C). Shown here are comparisons to both mock- and HCMV-infected telomerase immortalized fibroblasts (THFs; the parental background for WF28-71) and HFFs. Not surprisingly, given the very low level of pp71 IF staining (Fig. 6A) and transcript levels (Fig. 6B), we were unable to detect pp71 protein by Western blotting analysis of these cells (Fig. 6C, middle). Attempts to detect pp71 with an antibody (Ab) to the hemagglutinin (HA) tag on this protein were also not fruitful (Fig. S3A). To control for any long-term effects of

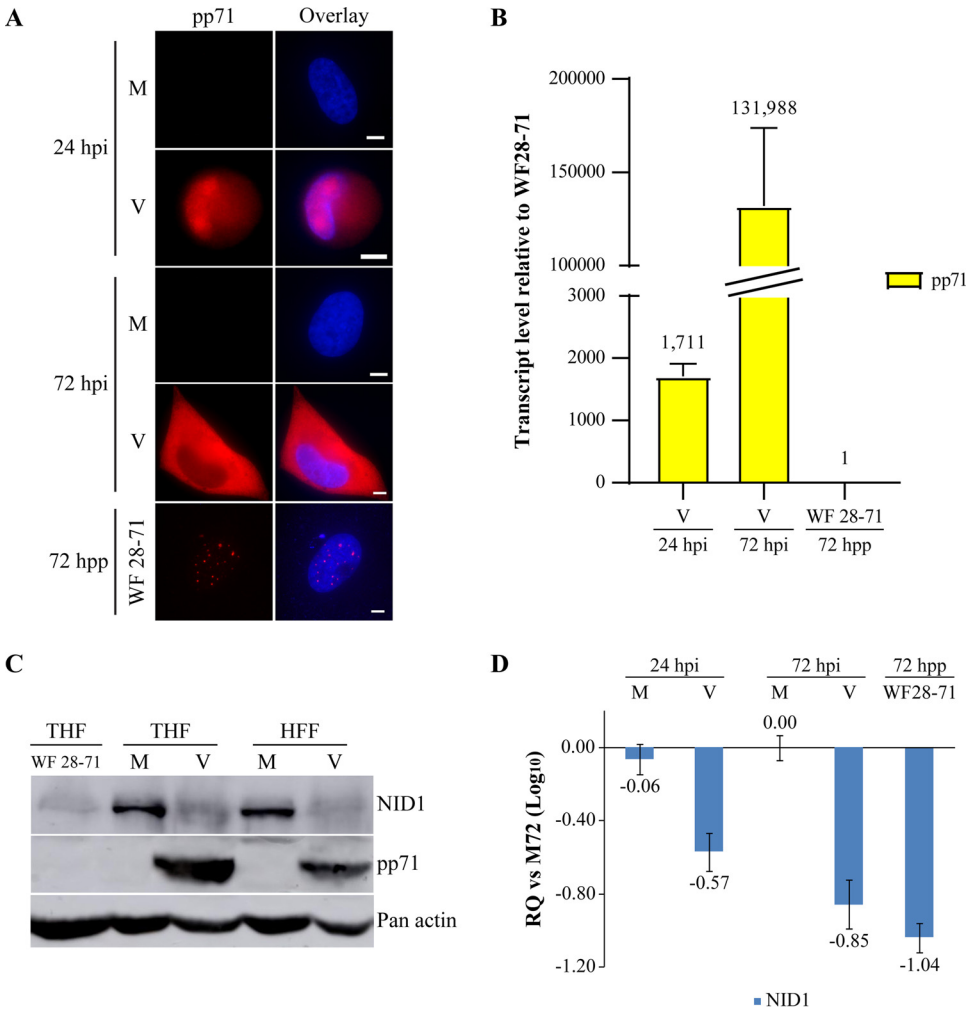

FIG 6 Long-term expression of a minute amount of pp71 downregulated NID1. (A) WF28-71 cells were stained for pp71 in comparison to HCMV-infected cells at 24 and 72 hpi. Small foci were observed in many WF28-71 cell nuclei; hpp, hours post plating. (B) RT-qPCR analysis to quantitate the relative levels of *pp71* transcripts in the WF28-71 cells (reference sample) versus those present during HCMV infection. (C) Western blotting of ss NID1 and pp71 levels in WF 28-71 cell lysates compared to mock- or Towne-infected THFs and HFFs at 72 hpi (18 μl). (D) RT-qPCR analysis determined the level of *NID1* transcripts in the WF28-71 clone in comparison to HCMV-infected HFFs at 24 and 72 hpi. Data are presented as changes relative to mock-infected cells at 72 hpi.

pp71 expression in these WF28-71 cells, which have been passaged extensively since their creation, we used the same expression plasmid (or the parental backbone) to create a new cell line in a completely different cell type. IPN2.3 cells are a telomerase-immortalized human Schwann cell line that expresses low levels of NID1. When the A5 clone expressing the pp71 construct was compared to a control line expressing the backbone plasmid, we again observed a decrease in the ss level of NID1 via Western blotting analysis (Fig. S3B). For comparison, mock- and HCMV-infected HFFs are also shown.

Having observed a dramatic decrease in ss NID1 levels, we next analyzed *NID1* transcript levels in the WF28-71 cells. As, or even more, dramatically, *NID1* transcription in the WF28-71 cells was decreased to a level comparable to, or greater than, that observed in HFF cells infected with HCMV for either 24 or 72 h (Fig. 6D). The presence of an almost infinitesimal but sustained amount of pp71 in the telomerase-immortalized fibroblasts (or in immortalized Schwann cells) created a void of NID1 within these cells.

Chromatin immunoprecipitation (ChIP) revealed that pp71 was bound to the cellular DNA. The tegument protein pp71 was clearly involved in the transcriptional regulation of *NID1*, but via what mechanism, particularly in light of minute quantities of pp71 being able to exert this control? Even though we had determined that

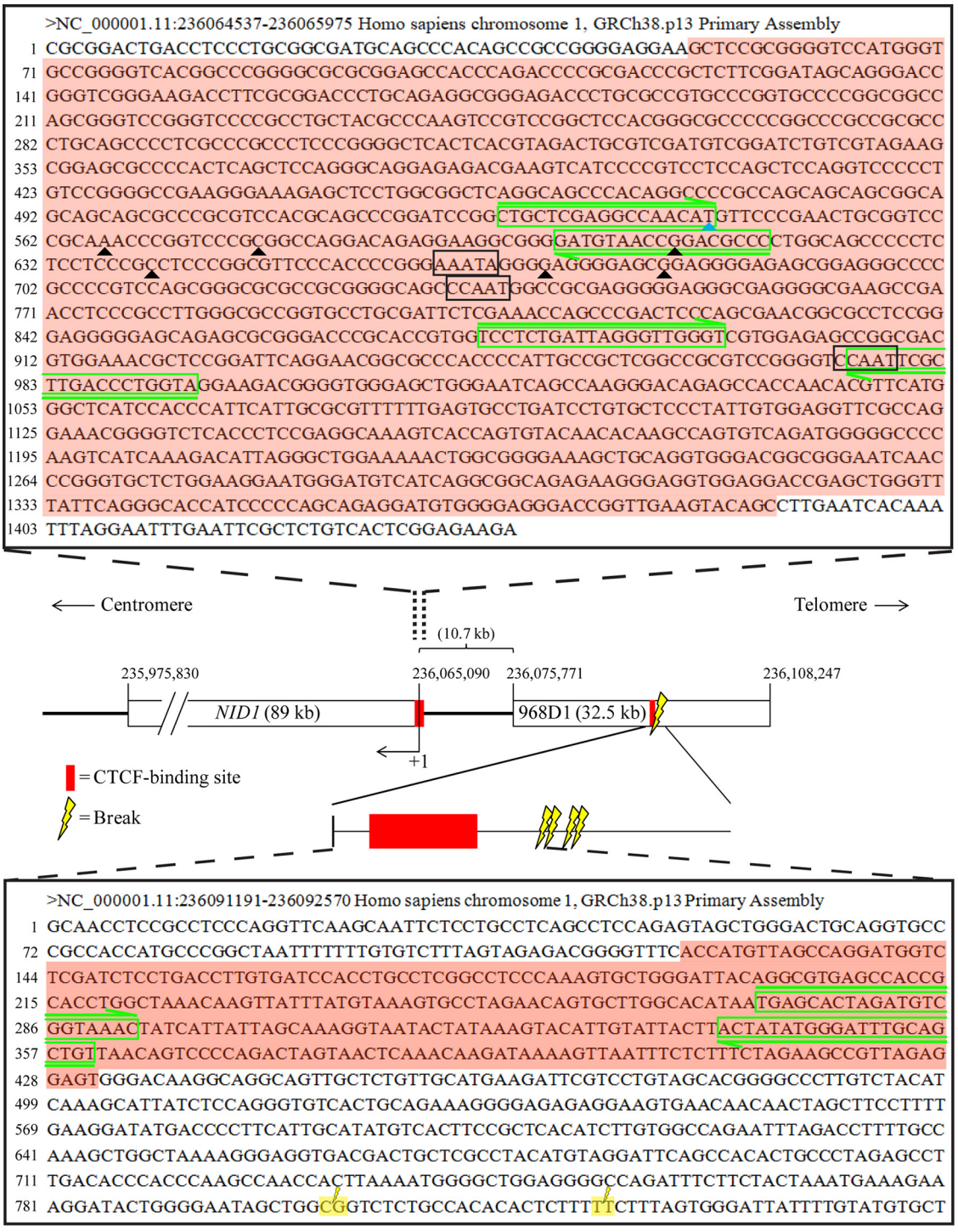

FIG 7 Predicted CTCF-binding sites were localized near the *NID1* promoter and 1q42 break sites. Genomic analysis using the Ensembl database revealed CTCF-binding sites (shaded in red) adjacent to both the *NID1* promoter region (upper sequence expansion) and the 1q42 break site region (lower sequence expansion). In the upper sequence, multiple FANTOM5-predicted transcription start sites are indicated by black triangles. The literature-defined noncanonical TATA variant TATTT sequence on the negative strand and the two canonical CCAAT motifs upstream of these transcription start sites are marked in black boxes (29). The translational start site is denoted with a blue triangle for reference. Primers used for ChIP analysis are boxed in green. The lower expanded sequence shows the 1q42 break site region (as in Fig. 1B), with the ChIP primers denoted in green. The first two LMPCR-defined break sites are shown for reference.

artificially introducing breaks equivalent to those induced by HCMV did not inherently cause ss NID1 downregulation (Fig. 1D and Fig. S1B), we reasoned that these HCMV-induced breaks were indicative of a direct interaction between virus protein(s) and the cellular DNA in this area. A closer examination of the sequences surrounding the break sites defined by LMPCR (lower expanded region in Fig. 7; break sites 1 and 2 are defined in yellow) and the literature-defined *NID1* promoter region (29) (upper expanded region in Fig. 7; canonical and noncanonical promoter-related sequences are boxed) revealed Ensembl-defined putative binding sites for the cellular regulatory protein CTCF (expanded sequences shaded in red in Fig. 7). The literature reports that many herpesviruses use the activity of CTCF to control the expression of viral gene products (e.g., to silence their expression [30–40]) and that CTCF is upregulated by HCMV infection (41, 42). We hypothesized that HCMV could also use CTCF, either alone or in combination with pp71, to control expression of *NID1* by binding to one or both of these regions. To test this hypothesis, we performed ChIP experiments, precipitating cross-linked chromatin with antibodies directed either toward CTCF or pp71 (see Materials and Methods for specifics). Precipitated DNA was then subjected to quantitative PCR (qPCR) experiments using primers (outlined in green in the expanded sequences in Fig. 7) designed to test for enrichment of binding to these two regions in infected samples compared to mock-infected controls.

We performed our initial ChIP analysis of binding to both the *NID1* promoter region and the 1q42 - defined break site region (shown schematically in Fig. 8A) at 24 hpi during HCMV infection, since we had previously observed clear transcriptional regulation of *NID1* expression at this time (3) (Fig. 6D). CTCF (red bars) and pp71 (blue bars) both demonstrated enriched binding in virus-infected lysates when normalized to mock-infected lysates (expressed as fold enrichment V/M) in both assayed regions after specific Ab precipitation (Fig. 8B). These enrichments all proved statistically significant when analyzed over multiple experiments. As we had also observed a similar level of transcriptional regulation during sole expression of Adpp71, we infected with this vector (or Adic as a control) and again assayed for binding of both CTCF and pp71 via ChIP at these two regions (at 48 hpi to allow for full expression of the transgene). Even in the context of only exogenous pp71 expression, both proteins showed enriched binding over Adic control lysates (expressed as fold enrichment Adpp71/Adic) at these two regulatory sites (Fig. 8C), albeit at somewhat lower levels of enrichment than those observed during HCMV infection. Although not quite reaching a level of statistical significance, pp71 binding to the *NID1* promoter ($P = 0.07$) and CTCF binding to the 1q42 break site ($P = 0.08$) were consistently increased in Adpp71-infected cells in all experiments performed.

Because the DSBs occurred very quickly (as early as 15 min pi), indicating almost instantaneous interaction with these regions (3), ChIP analysis was again performed after HCMV infection, this time extracting DNA after only 1 hpi to look for enrichment of both CTCF and pp71 at the two sites. Perhaps surprisingly, we observed enrichment of binding for both proteins (over mock-infected controls) at both sites at this very early time pi (Fig. 8D). Interestingly, a somewhat higher statistically significant enrichment occurred at the break site region for both proteins. Less enrichment was observed for both proteins at the *NID1* promoter at this very early time point, with somewhat higher levels of pp71 ($P = 0.055$) at this site. In all experiments performed at this very early time point, enrichment for pp71 was consistently higher at both sites.

Input pp71 and CTCF were colocalized in the nucleus. In our earlier work and in the broader literature (3, 20, 21), pp71 has been found in puncta initially after infection, with very rapid transport to the nucleus after virion deposition in the cytoplasm. Our ChIP experiments suggested that pp71 and CTCF might be complexed within the nuclear puncta at early times pi. We utilized an "extraction first" staining methodology that we have described previously (43–45). This procedure removes proteins that are not attached to the chromatin or scaffolding substructure of the nucleus prior to fixation, providing an unobstructed view of protein localization within this compartment. We then used confocal microscopy to localize pp71 foci (green), presumably "bound"

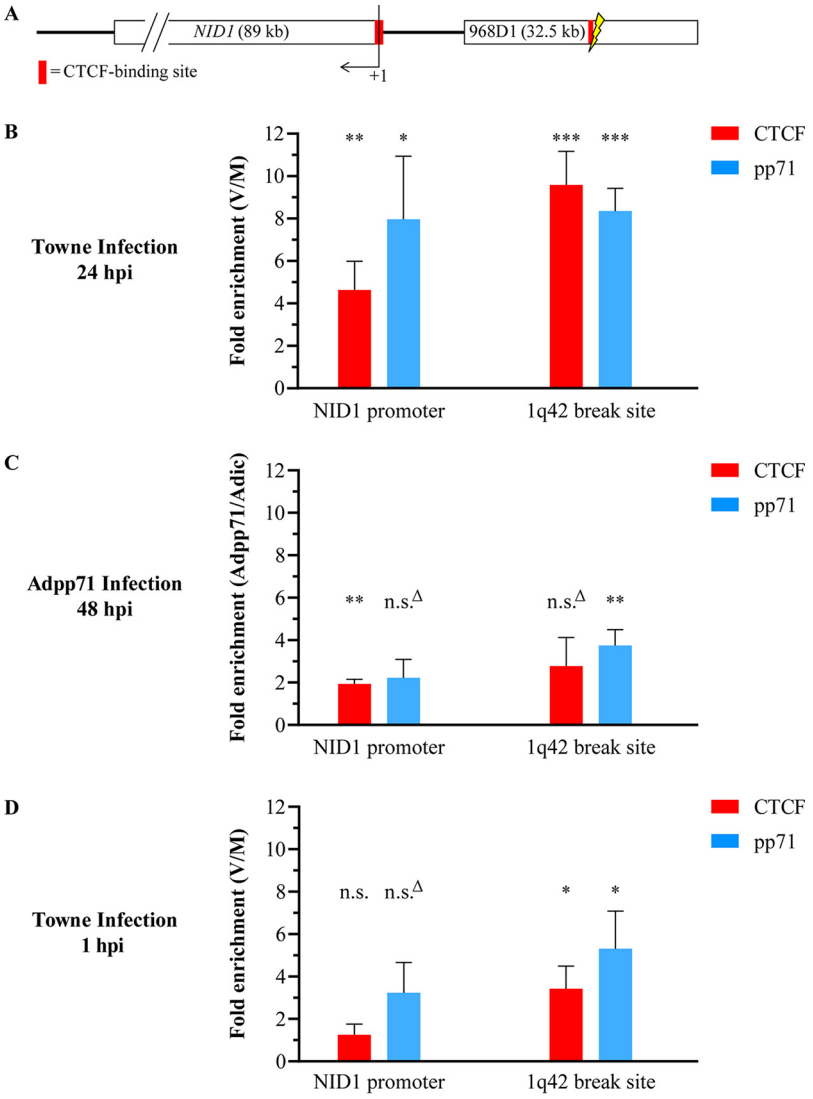

FIG 8 pp71 and CTCF were both bound to the *NID1* promoter and 1q42 break site region. (A) Diagram of the *NID1* promoter and the break site region of chromosome 1 showing the defined CTCF-binding areas being assayed for binding by pp71 and CTCF. HFFs were mock- or HCMV-infected at an MOI of 5 (B and D) or Adic- or Adpp71-infected at an MOI of 10 (C). Cells were harvested for ChIP (as described in Materials and Methods) at the indicated times pi. Chromatin was immunoprecipitated with antibodies to CTCF (red bars) or pp71 (blue bars). Enrichment of binding in the infected samples to the *NID1* promoter or the break site region was compared to the reference samples (mock or Adic) and expressed as fold enrichment V/M or Adpp71/Adic, respectively. Representative results are shown. Analyses represent an average of three replicates. Statistical analysis was performed to compare the data from multiple experiments to determine significance of enrichment.

to chromatin, and CTCF foci (red) at very early times pi (15 and 60 min) to determine whether there was any colocalization (Fig. 9). CTCF is a major transcriptional regulator of cellular genes; therefore, it was unsurprising to see many CTCF foci within mock- and virus-infected cells, with the latter having a somewhat larger number of foci (red puncta). This was not unexpected given HCMV infection's reported upregulation of CTCF expression (41, 42). pp71 puncta were observed within the nuclei of infected cells, even at the earliest time point of 15 min pi (Fig. 9, middle row). Quite astonishing were one or two clearly colocalized pp71 and CTCF foci in infected cell nuclei almost immediately after infection. Colocalized foci are delineated by white arrows in the merged panels in Fig. 9, which are enlarged in the adjacent panels. Multiple images were scored at both 15 and 60 min pi for both total pp71 foci and those that were

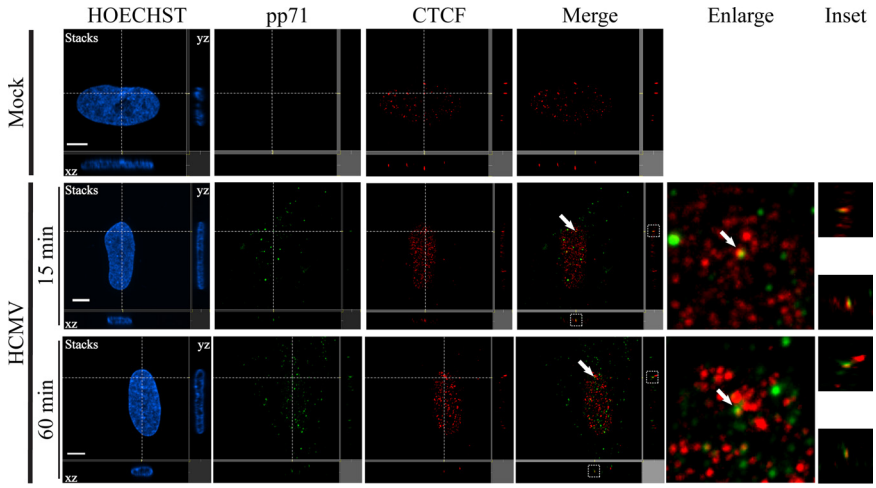

FIG 9 pp71 and CTCF colocalized in a small number of nuclear foci at extremely early times pi. Infected cells were harvested at 15 or 60 min pi. Cells were harvested and processed using "extraction first" methodology (as described in reference 44). Cells were stained for pp71 (green) and CTCF (red) and analyzed by confocal microscopy. The large views (upper left regions of each image) are combined confocal stacks of an individual cell. Both *xz* and *yz* represent a single section captured at the dashed crossing lines perpendicular to the large view. Merge and enlarge columns show both pp71 and CTCF. White dashed boxes in *xz* or *yz* in the merge column are enlarged in the inset column, showing the colocalization of pp71 and CTCF.

colocalized with CTCF (Fig. S4). Both time points showed an average of ~115 pp71 foci within their nuclei, with each cell consistently containing an average of three pp71/CTCF colocalized puncta. Taken together, these early ChIP and localization data indicate association of these two proteins beginning very rapidly after infection.

CTCF was necessary for pp71-directed NID1 regulation. The binding of CTCF and pp71 at the *NID1* promoter and the CTCF binding site adjacent to the chromosome 1 break sites combined with the colocalization observed within infected cell nuclei suggested that these proteins were interacting to influence *NID1* transcription. Therefore, it stood to reason that depletion of CTCF from the cellular milieu would diminish the ability of pp71 to regulate *NID1* expression within the cells. To address this possibility, we knocked down CTCF using a lentiviral short hairpin vector (shCTCF) as we had done previously (35). A lentiviral short hairpin scramble vector (shScramble) served as a control of the lentiviral infection. Fig. 10A shows the efficient knockdown (KD) obtained using this lentiviral delivery system. HCMV infection induces an increase in the steady-state level of CTCF (41, 42), which could potentially obfuscate any ramification that removal of CTCF from the cell might affect NID1 ss levels. Therefore, to avoid this issue, we used Adpp71 infection (at an MOI of 2) to introduce pp71 into the CTCF-KD HFFs. Ad-infected cells were harvested at 72 hpi for Western blotting and RT-qPCR analyses. CTCF levels were not affected by the introduction of just pp71 within the CTCF KD cells (Fig. 10B, middle); however, only in the presence of CTCF did Adpp71 infection regulate ss NID1 levels (compare NID1 levels in shScramble to shCTCF lanes; Fig. 10B, top). As could be predicted (41, 42), HCMV infection in CTCF-KD cells increased CTCF levels within them, negating any effects on ss NID1 levels (Fig. S5). *NID1* transcription was also recovered in the absence of wild-type levels of CTCF (Fig. 10C, compare the Adpp71 decrease observed in the shScramble-treated cells to that observed in shCTCF-treated cells). These results confirm that cellular CTCF was a necessary component for pp71, and HCMV, to downregulate *NID1* transcription and, ultimately, ss NID1 protein levels within infected cells.

DISCUSSION

Recreation of the DSBs induced by HCMV in the cellular DNA did not downregulate ss NID1. Since identifying specific DSBs induced by HCMV infection more than 20 years ago, which occur rapidly in every cell type tested, we have believed that their

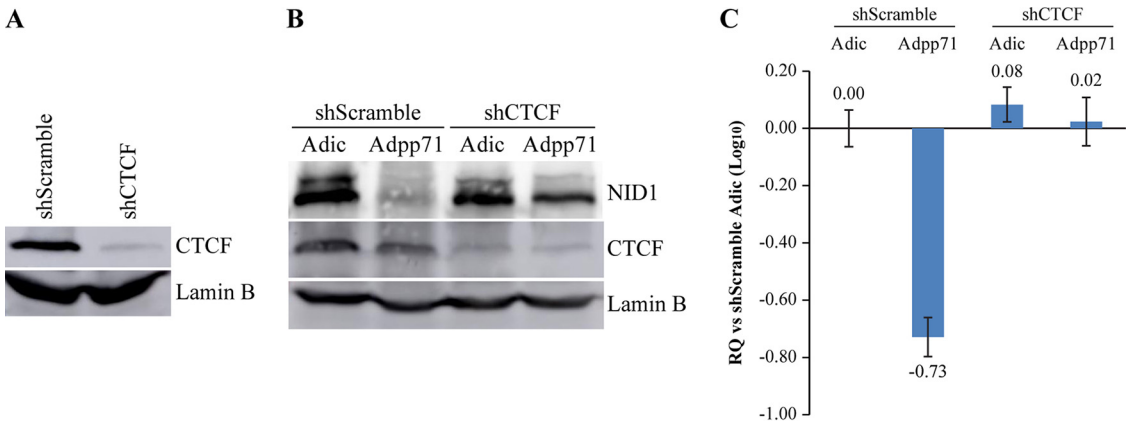

FIG 10 CTCF was essential for pp71 to downregulate NID1. CTCF was knocked down using a lentiviral short hairpin RNA vector (shCTCF). A lentiviral short hairpin scramble vector (shScramble) served as a control for the lentiviral infection. (A) Steady-state CTCF was substantially knocked down in cell lysates (20 μL) of HFFs after lentiviral transduction and puromycin selection. These cells were then infected with Adpp71 (or control Adic) at an MOI of 2 to introduce pp71. These cells were harvested at 72 hpi for Western blotting (20 μL of lysate) (B) and RT-qPCR analyses for *NID1* (C). The latter used the normalized transcript level within the Adic-infected shScramble cells as the reference sample.

inherently imperfect repair was linked to pathologies observed in congenital infection. Our suspicions were supported by the persistence of breaks over the time course of infection (2, 3) and HCMV's distinct interactions with the DNA damage/repair machinery, which essentially shunts repair preferentially to the viral DNA (46–48).

Fine mapping of the 1q42 break sites via LMPCR revealed that cleavage was not an enzymatic-type event but rather the induction of fragility within the region. We mapped four distinct break sites in this study; however, introduction of equivalent breaks via CRISPR in six separate samples within the same region, which allow for the "misrepair" of these breaks inherent to the nonhomologous end joining (NHEJ) process, failed to induce any changes to the ss NID1 level. The highest percentage of breaks observed by FISH analysis in infected samples was ~30% at any given time pi (3), while some of our CRISPR constructs achieved 80 to 90% breakage/mismatch introduction. Therefore, we no longer believe that the break activity or its misrepair is responsible for the ss NID1 level decrease or any pathologies that NID1's absence may induce.

When we discovered these distinct interactions of HCMV with the DNA leading to site-specific damage, we were struck by HCMV being one of only two DNA viruses that interact with the cellular chromatin at particular loci, the other being the oncogenic adenovirus type 12 (Ad12) (49–51). The work of Silvia Bacchetti's group (52) defined the necessity of Ad E1B-55K (and its activation of p53) for the induction of these sites of fragility. Importantly, the Ad delivery vectors utilized in this study do not encode E1B-55K. It is noteworthy that each of the four defined sites are regions corresponding to a cluster of small abundant structural RNAs, three of which (*RNU1*, *RNU2*, and *RN5S*) are highly transcriptionally active (as reviewed in reference 53). Work from Alan Weiner's laboratory showed that these three loci each require the activity of the Cockayne's syndrome B (CSB) DNA repair protein for proper condensation in preparation for mitosis (54). Interference of this CSB interaction via E1B-55K-initiated p53 activation leads to a lack of condensation of the chromatin and induction of fragility by Ad (55). E1B-55K does not interact directly with the loci. HCMV-induced fragility is via an entirely different mechanism and is a by-product of the binding of the viral protein pp71, in conjunction with CTCF, to the cellular DNA to downregulate ss NID1, presumably providing the virus a life cycle advantage.

Several viral proteins contributed to downregulation of ss NID1 levels, each contributing in a different manner. Because the interaction with the 1q42 region is initiated so quickly, we began our analysis with virion-delivered and rapidly synthesized viral proteins. We found that regulation of NID1 occurred via both input components (as

determined by +UV infections) and *de novo* synthesized proteins (by exogenous delivery of IE1). Expression of individual tegument proteins revealed roles for both pp71 and UL35 in ss NID1 regulation as well as a role for the immediate early protein IE1. We suspect that to achieve the level and speed of regulation observed after HCMV infection, all the players may need to be expressed within the cell. For instance, delivery of just virion components produced less robust transcriptional regulation of *NID1* than permissive infection and essentially no proteasomal regulation. The incomplete recapitulation of NID1 downregulation by short-term expression of individual viral proteins may also indicate that additional viral proteins contribute to the regulation of this important basement membrane protein, which appears to be paramount to the virus given the effort it exerts toward its removal.

pp71. pp71 is a multifunctional HCMV tegument protein with extensive roles in regulating the intracellular space to better promote efficient viral gene expression and replication. Those roles are initiated almost immediately upon virion entry into the cell and include interaction with the host-encoded antiviral factors DAXX and ATRX (20, 56–59) and the more recently discovered BclAF1 (11). pp71 regulates DAXX and BclAF1 via proteasomal degradation; however, we found no such role for pp71 in the HCMV-induced downregulation of NID1. pp71 also inhibits deposition of chromatin on incoming genomes (via its interactions with DAXX and ATRX) and may derail cellular repression of the major immediate early promoter (MIEP) (42). It has been known for several years that pp71 stimulates the expression of a wide range of promoters (including the MIEP) in a sequence-independent manner (20, 60, 61). In addition, pp71 has been shown to bind and influence the translation of both viral and cellular mRNAs (62), although the RNA-binding region within pp71 has not been mapped. *NID1* mRNA was not in the list of regulated mRNAs in this study. To date, no data have been presented demonstrating the binding of pp71 to any sequence of DNA of either cellular or viral origin. To our knowledge, our study is the first to find direct binding of pp71 to the cellular DNA, in conjunction with CTCF, leading to transcriptional control of a cellular protein.

Both published (14) and unpublished (J. Kerry, personal communication) data suggest that pp71 interacts with several other cellular proteins to accomplish its viral functions. Of particular interest to our findings are pp71's potential interactions with PARP-1, *N*-acetyltransferase 10, histone H1.3, and histone macro H2A.1 (J. Kerry, personal communication). These interactions are all potentially important for modifying the chromatin to access the DNA, which could also be relevant for pp71's interactions with CTCF. It is tempting to speculate that pp71 interactions with PARP-1 might parallel the situation that we have observed after Epstein-Barr virus (EBV) infection, where we have shown that PARP-1 interacts with the EBV genome and the EBNA1 protein (63) and that PARP-1 also regulates CTCF binding across the EBV genome (64, 65).

UL35. An additional virion-delivered component, UL35, was found to regulate ss NID1 levels and accounts for at least some proportion of the proteasomal degradation observed after infection. The RNA transcript for *UL35* and the smaller C-terminal-encoded *UL35A* were first described by Liu and Biegalke (24). Intriguingly, the smaller transcript initiates from an internal start site and encodes an identical stretch of amino acids yet appears to function quite differently. Full-length UL35 is produced beginning at 48 hpi and is packaged within the viral tegument, making it a component of input virions and dense bodies. Fabits and colleagues (66) showed that incoming UL35 traffics efficiently to the nucleus by 1 hpi, making it a prime candidate for early interactions with NID1. By contrast, UL35A is not present within the virion but is transcribed with IE kinetics, being first observed at approximately 4 hpi. As shown in Fig. 3C, UL35 full-length protein is the predominant form present within AdUL35-infected cells. Interestingly, our AdUL35-expressing cells also expressed UL35A in quite similar quantities to those found during HCMV high-MOI infections (compare levels of UL35A in lanes 2, 3, and 4 in Fig. 3C). The literature is conflicting as to the synergistic versus antagonistic effects of UL35 and UL35A with respect to interactions with pp71. Although several papers show a synergy between UL35 and pp71 (11, 23,

67), the literature also points to antagonism of pp71 functioning (24) and localization in the presence of UL35A (23).

We have been unable to fully answer whether both forms of the protein need to be present to affect ss NID1 levels. We found that sole expression of UL35A did not influence ss NID1 levels but have not been able confirm or deny whether UL35 acts in concert with its smaller subunit or not in regulating ss NID1. Although they are contiguous in their encoded amino acids, there are disparities between the functions ascribed to full-length UL35 versus the smaller UL35A. Some papers describe similar functions of the two proteins (66, 68), while others have found that only the full-length protein can enact change (23, 25). Relevant to our observations, Salsman and colleagues (23) found in transfected cells that although USP7 coprecipitated with both UL35 and UL35A, the Cullin 4A-associated E3 ubiquitin ligase components DCAF1, DDB1, and DDA1 only associated with full-length UL35. These results strongly suggest interaction between UL35 and the proteasomal degradation machinery. In very preliminary experiments, infection of UL35A-expressing cells required a lower concentration of AdUL35 (MOI of 10) to affect the same decrease in ss NID1 levels as an MOI of 25 when expressed alone (Fig. S6 in the supplemental material). This could help to explain why tegument-delivered proteins alone were not capable of proteasome-mediated degradation of NID1 (as seen in Fig. 2H), as UL35A would not be present during these infections. Perhaps also playing a role is the inevitable decline in input tegument proteins at this late time (48 hpi) after UV-inactivated virus infection. Future experiments will be directed at disentangling this question.

IE1. We also found that *de novo*-expressed IE1 downregulated ss NID1 levels. It has long been known that the viral immediate early proteins IE1 and IE2 regulate the transcription not only of viral promoters, including their own, the MIEP, but also multiple cellular promoters (as recently reviewed in reference 69). The IE1 protein regulates cellular gene expression via epigenetic regulation of chromatin and also regulates both intrinsic and adaptive immunity (as reviewed in reference 69). We found no evidence that IE1 regulated *NID1* transcription. The literature points to IE1 also being able to regulate the protein levels of a few cellular genes via proteasomal degradation, including the antiviral protein SP100 (70, 71) and the neurodevelopmental marker Hes1 (71). The latter paper showed that IE1 could act as an E3 ubiquitin ligase, although this does not appear to be the method that IE1 uses to regulate ss NID1 levels. How IE1 accomplishes this task will require further exploration.

NID1 is one of a limited number of cellular proteins regulated by multiple viral gene products and pathways. Large-scale transcriptomic and proteomic analyses have had some success in revealing cellular components regulated by multiple viral proteins (and/or RNAs) acting in concert (as reviewed in reference 1). For instance, Nobre et al. (14) revealed that during viral infection, the binding of Cullin4 E3 and its adaptors by UL145 and RL1 leads to the degradation of the cellular protein HLTF. The only other detailed report comes from Lee and colleagues (11), who found that BclAF1 levels were regulated by pp71, UL35, and the viral microRNA UL112A. Early regulation was proteasomally mediated, with later regulation coming through translational repression. Interestingly, although transiently expressed pp71 was capable of binding to BclAF1, it could not degrade it by itself, and, although UL35 was capable of degrading BclAF1 on its own, wild-type degradation was only achieved with coexpression of both proteins.

It is perhaps not surprising that pp71, UL35, and IE1 were found to be working in concert to regulate NID1, as they have been shown to interact in the past. It was shown that both pp71 (60) and UL35 (24) could aide in the transactivation of the MIEP mediated by IE1. Chau and colleagues (72) found that pp71-mediated aid in IE1 transactivation extended to the viral *US11* promoter and demonstrated that this regulation required the ATF and CREB sites within the *US11* promoter.

Several studies have reported protein-protein interactions between pp71 and UL35, first defined by Schierling and colleagues (67) in yeast two-hybrid studies and reiterated in infected cells, with the binding domain on UL35 mapped to amino acids 447 to

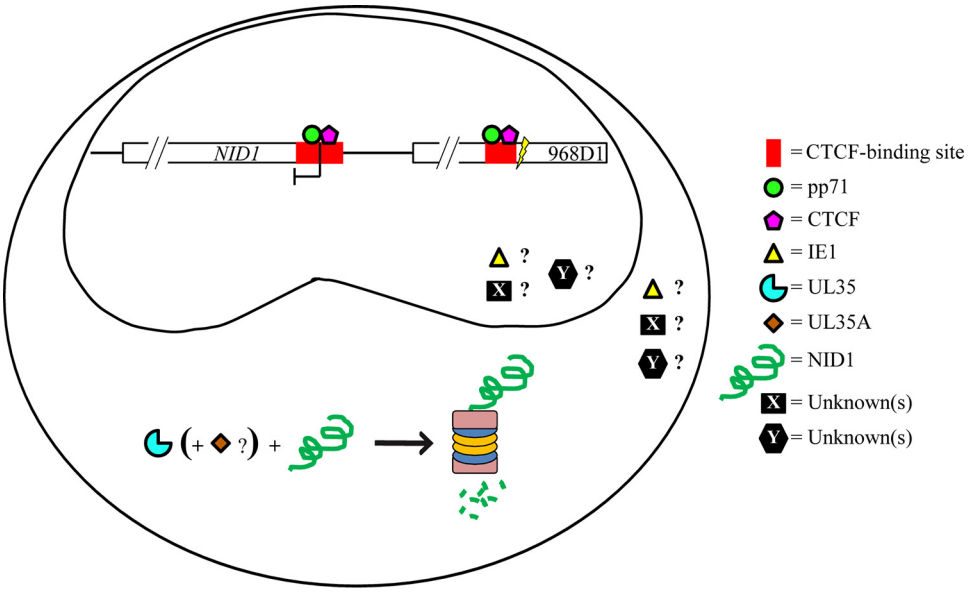

FIG 11 Model of NID1 regulation during HCMV infection. During HCMV infection, pp71 and CTCF are bound to the *NID1* promoter and, as a consequence, inhibit *NID1* transcription. These two proteins are also bound to the 1q42 break site region. Breaks may occur due to torsion on the DNA caused by interaction between these two sites. Another tegument protein, UL35, potentially in conjunction with UL35A, leads to NID1 protein degradation via the proteasome. How IE1 is involved in ss NID1 downregulation is yet to be determined. There could also be additional unknown proteins (X and Y) involved in the downregulation of NID1 in either the nucleus or the cytoplasm.

566, which also encompasses UL35A. This interaction, along with all other viral protein-protein interactions within the infected host cell, have been mapped in a large proteomic analysis (14). Interestingly, this paper described that pp71 had 15 interactions (viral=pp65, pp150, UL35), UL35 had 3 interactions, and UL123 (IE1) had 27 separate interactions. No clear protein-protein binding interactions were observed between a viral protein and NID1 directly in this study. There were also no direct interactions observed between pp71 (or UL112A microRNA) and NID1 in a study performed by Lee and colleagues (11). These latter pulldown studies were performed in HeLa cells, so the NID1 protein may not have been expressed at sufficient levels at the outset of the experiment.

While we have shown the capacity of three viral proteins to regulate ss NID1 levels within infected cells, the short-term introduction of any one of these individual proteins did not completely replicate the effect of HCMV-permissive infection on either transcription or proteasomal degradation. Therefore, we believe that there may be other viral proteins involved in HCMV's interaction with NID1. The Weekes lab's 2019 paper (14) identified several other viral proteins that interacted with the ubiquitin/proteasomal machinery, including UL36 and UL102, that also interact with ubiquitin, including UL42, UL30a, UL102, and UL36, which all interact with the ubiquitin protein transferases, and UL145, RL1, UL42, UL30a, UL102, UL147, and UL36, which all interact with the ubiquitin conjugation pathway. In addition, there are other viral proteins that have been shown to have transactivation functions, namely, UL69 (73) and the TRS1/IRS1 locus-encoded proteins, which we were unable to express efficiently in our studies (74, 75). It is possible that any of these proteins could contribute to HCMV's assault on NID1. A model of the players we have identified and their roles in decreasing the ss levels of NID1 within the infected cell (along with potential other still unidentified players) is shown in Fig. 11. Once again, this points to the seemingly distinct importance for the virus to target this BM protein. As our original paper posited (3), this may very well be to increase the capacity for viral dissemination throughout the infected individual.

Regulation of ss NID1 levels required a nominal amount of pp71. Our data indicated that the presence of an incredibly small amount of pp71 within cells over an extended

period of time, as in the WF28-71 cells or newly created IPN2.3 A5 cells, induced the complete absence of ss NID1 protein, presumably via its long-term downregulation of transcription. Transcriptional analysis found that the level of *pp71* transcript present in these cells was 1,700 times less than that present at 24 hpi in a permissively infected cell, and yet the same degree of NID1 downregulation was present. We speculate that the continual production of very low levels of pp71 in these cells permits continual binding to the *NID1* promoter (and the adjacent 1q42 break site region) by pp71 and CTCF. We contend that under such conditions, essentially no *NID1* transcript is ever made, and, subsequently, no new NID1 protein is translated. The few small pp71 puncta that we observed in WF28-71 cells could be these binding sites. Importantly, according to current literature, latently infected cells express *pp71* transcripts (76–78), which could, in theory, continuously downregulate *NID1* expression. Whether low-level expression of pp71 in latently infected cells plays a role in the developmental issues that we see in congenitally infected infants is a question that we are attempting to answer using a cerebral organoid model.

HCMV coopts CTCF to aide in regulation of *NID1*. Herpesviruses use control of the insulator protein CTCF, making it unsurprising that this cellular protein contributes to the regulation of *NID1*. CTCF regulates/insulates lytic and latent genes during EBV and herpes simplex virus (HSV) infection (30–40). Recent evidence suggests that CTCF binding sites on the HSV-1 genome are regulated differentially and independently to help control the lytic/latent switch (39). Although it has been known for several years that CTCF levels are upregulated after HCMV-permissive infection and that the protein downregulates HCMV *IE1/2* transcription (42), very recent data from John Sinclair's lab show that CTCF is also upregulated in latently infected monocytes (41). This increase in CTCF is regulated by the presence of US28. The authors showed that CTCF binds to both the *MIEP* and *S100A8/A9* promoters to downregulate transcription during latency and that sole expression of US28 accomplished the same repression. The authors did not explore whether US28 was also bound to these promoters, as we have observed with pp71 regulation in conjunction with CTCF. Future experiments will determine whether pp71 recruits CTCF to the two sites that we have defined. It is tempting to speculate that the small number of pp71/CTCF colocalized foci that we observed exceedingly early pi represent pp71 and CTCF bound to the two loci defined here. We are also keen to determine whether pp71 may bind to other regions of the cellular genome to initiate regulation of other important proteins, with or without the additional required presence of CTCF. pp71 binding may be similar to EBV EBNA1 and Kaposi's sarcoma-associated herpesvirus (KSHV) LANA protein interactions with the cellular genome (79, 80). Studies are underway to determine the possible extent to which pp71 binds to both the cellular and viral genomes during infection.

In this study, we have uncovered key HCMV viral proteins responsible for the regulation of the important basement membrane protein NID1. We have also found that the tegument protein pp71 binds directly to the cellular DNA, in conjunction with the cellular insulator protein CTCF, thereby, presumably, regulating *NID1* transcription. To our knowledge, this is the first time pp71 has been shown to directly interact with DNA. We have also shown the direct utilization of, and necessity for, CTCF in HCMV-induced NID1 downregulation.

MATERIALS AND METHODS

Cells and culture conditions used. Primary human foreskin fibroblasts (HFFs; a gift from S. Spector, University of California, San Diego) and telomerase-immortalized human fibroblasts (THFs; a gift from V. DeFilippis, Oregon Health and Science University [OHSU] [28, 81]) were propagated in Earle's minimal essential medium (MEM) supplemented with 10% heat-inactivated fetal bovine serum (FBS), L-glutamine (2 mM), penicillin (200 U/mL), streptomycin (200 μg/mL), and amphotericin B (1.5 μg/mL). HEK 293T cells (for lentivirus and retrovirus propagation; ATCC, CRL 3216), HEK 293A cells (for Ad propagation; ATCC, CRL 1573), IPN2.3 telomerase-immortalized human Schwann cells (a gift from P. Wallace [82]), and pp71-expressing fibroblasts (WF28-71; a gift from W. Bresnahan [28]) were all maintained in Dulbecco's MEM (DMEM) supplemented with 10% heat-inactivated FBS (15% for WF28-71), L-glutamine (2 mM), penicillin (200 U/mL), and streptomycin (200 μg/mL). All cells were grown in humidified incubators maintained at 37°C and 5% CO_2.

To produce the A5 clone, the WF28-71 plasmid (expressing pp71 [28]) was introduced into IPN2.3

TABLE 1 LMPCR primers

Name	Sequence	Biotin
1q42-1F	5′-GCCTAGAACAGTGCTTGGCAC-3′	Yes
1q42-2F	5′-CACGGGGCCCTTGTCTACATCA-3′	Yes
L1	5′-CGAGTTCAGTCCGTAGACCATGGAGATCTGAATTC-3′	No
L2	5′-GAATTCAGATCTCC-3′	No
LN1	5′-CGAGTTCAGTCCGTAGAC-3′	No
LN2	5′-GTAGACCATGGAGATCTGAATTC-3′	No
1q42-1N1	5′-GAGCACTAGATGTCGGTAAACTATC-3′	No
1q42-2N1	5′-GCATTATCTCCAGGGTGTCACT-3′	No
1q42-1N2	5′-GGATTTGCAGCTGTTAACAGTCC-3′	No
1q42-2N2	5′-GCAGAAAGGGGAGAGAGGAAGTG-3′	No

cells via nucleofection (Amaxa Nucleofector II, 4 μg of DNA, program A-033). Cells were selected in G418 (800 μg/mL) under limiting dilution conditions to allow for outgrowth of clones. Single clones were isolated, amplified, and screened via immunofluorescence (IF) and real time quantitative-PCR (RT-qPCR) for the presence of pp71. The backbone plasmid WF28 was also introduced into IPN2.3 cells, followed by selection in G418 to produce a pooled population of control cells.

Viruses used. The Towne strain of HCMV was obtained from ATCC (VR 977) and propagated under standard conditions (83). An Ad vector-based system was used to exogenously express specific viral gene products following standard protocols for propagation and titering of viral stocks (84, 85). Viruses encoding pp71 (Adpp71) and pp65 (Adpp65) and a control backbone vector (Adic; all gifts from R. Kalejta, University of Wisconsin, Madison [86]) and viruses encoding IE1 (AdIE1) and IE2 (AdIE2) and a transactivator protein (AdTrans; gifts from D. Streblow, OHSU [27]) were all used to infect HFFs at the indicated MOIs. AdUL35 was constructed in our laboratory using the AdEasy system, as previously described (87). Briefly, the entire UL35 cDNA sequence was excised from pCMV3FC (a gift from L. Frappier [23]) using XhoI and XbaI and cloned into pAdTrack-CMV (Addgene, 16404) between these same sites. Then, the protocol described in He et al. (87) was followed for generation, growth, and screening of potential clones. Plaque purification was performed to enrich for 1:1 green fluorescent protein (GFP)/UL35 expression in the chosen clone prior to large-scale propagation.

Infection/transduction conditions. (i) HFF infections with HCMV Towne. G_0 synchronization was performed via serum starvation as previously described (88). Cells were trypsinized, counted, and reseeded at a lower density onto plates in complete MEM. After allowing 2 h (unless specified otherwise) for attachment, cells were infected at an MOI of 5 with HCMV or conditioned medium (CM). At 4 hpi, medium was replaced with fresh complete medium, and cells were harvested at the indicated times pi. Experiments using UV-inactivated HCMV (or CM) were performed as previously described (2). Briefly, a quantity of virus stock (or CM) corresponding to an MOI of 5 was irradiated in a UV Stratalinker 1800 at a dose of 4,000 J/m^2. After UV irradiation, 5 mM sodium pyruvate (Lonza, 13-115E) was added to scavenge free radicals before transfer onto cells. At 4 hpi, medium was replaced with fresh complete medium containing 5 mM sodium pyruvate for additional scavenging, and cells were harvested at the indicated times pi. In experiments involving inhibition of proteasomal activity, 0.5 μM MG132 (Tocris Bioscience, 1748) or DMSO (control) was added to plates at 4 hpi, as previously described, and cells were harvested at the indicated times pi (3). The literature shows that if performed during a high-MOI infection, this level of MG132 does not affect IE gene expression (89) and is not toxic to the cells.

(ii) HFF infections with adenoviruses. For Ad infections, G_0-synchronized cells reseeded in a 10-cm plate (as described above) were infected at room temperature with the indicated Ad vector at the indicated MOI for 30 min in 0.5 mL of phosphate-buffered saline (PBS) containing 0.01% $CaCl_2$ and 0.01% $MgCl_2$, with intermittant rocking. An additional 7 mL of growth medium was added before incubation at 37°C for the indicated length of time prior to harvest and analysis.

(iii) Lentivirus/retrovirus production and transduction to create pooled populations. Lentiviruses/retroviruses were generated by transfection of HEK 293T cells with a plasmid encoding the gene of interest (4 μg) along with 4 μg of a packaging plasmid (psPAX2, Addgene 12260, for lentivirus production or pMDgagpol [90] for retrovirus production) and a vesicular stomatitis virus G protein-coding pseudotyping plasmid (4 μg; pMD2.G, Addgene 12259) using Lipofectamine 2000 or 3000 (Thermo Fisher Scientific, 11668030 and L3000001, respectively) as previously described (3). Transduction of cells and selection of puromycin-resistant pools were performed also as previously described (3). To express HCMV UL35A, plasmid pBJ395 (a gift of B. Biegalke [24]) was used. To knock down CTCF, a combination of silencing plasmids shCTCF.1 and shCTCF.2 (Sigma-Aldrich, TRCN0000218498 and TRCN0000230191, respectively) were used. An shScramble plasmid (Addgene, 1864) was used as a control in the latter experiments.

(iv) AdUL35 infection of UL35A-expressing cells. HFFs were infected with UL35A-expressing retrovirus and selected in puromycin as described above. After allowing 24 h for recovery from selection, cells were superinfected with AdUL35 (or Adic) as described above and harvested for analysis of ss NID1 levels after 72 hpi via Western blotting.

Ligation-mediated PCR (LMPCR). Nested LMPCR was performed as described by Kong and Maizels (15) using HFF cells mock- or Towne-infected at an MOI of 5. Genomic DNA was extracted from cells harvested at 1 hpi. Note that all primers used for LMPCR are listed in Table 1.

(i) Primer extension. Biotinylated primers (1q42-1F or 1q42-2F) were annealed to extracted DNA by

mixing 4×10^3 cell equivalents of DNA with 0.6 pmol biotinylated primer and 1× NEB2 buffer (NEB) in a 15-μL reaction volume. Reactions were heated at 95°C for 3 min and then 58°C for 30 min. Primer extension was carried out at 37°C for 30 min following the addition of 9 μL of a mixture containing 0.25 mM of each dNTP and 7.5 U Klenow (NEB, M0210S). Reactions were stopped by adding 6 μL of cold Tris-Cl, pH 7.7, and heat inactivating at 75°C for 20 min.

(ii) Linker ligation. L1 and L2 primers were annealed to form blunt-ended duplex DNA linkers by mixing 20 μM of each primer in 250 mM Tris-Cl, pH 8.0, heating to 95°C for 5 min and 70°C for 1 min, and ramping down to 4°C at a rate of 0.4°C/min. Aliquots were stored at −20°C. Ligation reactions were performed by adding 45 μL of ligation mixture (1× ligation buffer, 0.1 mM preannealed linker, and 400 U of T4 DNA ligase [NEB, M0202S]) to the product of the extension reaction and incubating overnight at 16°C. Streptavidin beads (300 μg) were washed in 2× wash buffer (10 mM Tris-Cl, pH 7.3, 1 mM EDTA, 2 M NaCl, and 0.02% Tween 20) and resuspended, and a 1:1 volume was added to the ligation reaction. Binding was performed at 43°C for 1 h, with mixing every 5 min before washing twice with 2× wash buffer and once with 10 mM Tris-Cl, pH 7.5.

(iii) Nested PCR. The reaction volumes were 50 μL for each round. The washed beads, with bound extension-ligation products, were resuspended in 40 μL of Tris-Cl, pH 7.5. To one quarter of the resuspended beads, 100 nM primer LN1 (nested primer, internal to linker L1) and 1q42-1N1 or 1q42-2N1 (nested primer, internal to biotinylated primers) was added, plus an equivalent volume of HotStart-IT *Taq* DNA polymerase (USB, 71195). For the first round of PCR, the following conditions were used: 1 cycle (95°C for 2 min, 55°C for 4 min, and 72°C for 3 min), 2 cycles (95°C for 45 s, 55°C for 1 min, and 72°C for 2 min), and 1 cycle (72°C for 7 min). Beads were pelleted, the reaction mixture was transferred to a new tube, and the PCR continued under the following conditions: 1 cycle (95°C for 2 min, 55°C for 4 min, and 72°C 3 min), 28 cycles (95°C for 45 s, 55°C for 1 min, and 72°C for 2 min), and 1 cycle (72°C for 7 min). For the second round of PCR, each reaction contained 2 μL of the first-round PCR products, 400 nM primer LN2 (nested primer, internal to linker LN1), and 1q42-1N2 or 1q42-2N2 (nested primer, internal to 1q42-1N1 or 1q42-2N1) and an equivalent volume of HotStart-IT *Taq* DNA polymerase. PCRs were performed under the following conditions: 1 cycle (95°C for 4 min), 35 cycles (95°C for 45 s, 62°C for 1 min, and 72°C for 2 min), and 1 cycle (72°C for 30 min). Products were visualized on a 1.5% agarose gel.

(iv) Sequencing and break site determination. Second-round nested PCR products were cleaned using GeneJET PCR purification columns (Thermo Fisher, K0701). Products were sequenced with primers LN2 and either 1q42-1N2 or 1q42-2N2 for products amplified from biotinylated primers 1q42-1F and 1q42-2F, respectively. Sequences were compared to the bridging clone (968D1) via the NCBI BLAST function to determine break sites.

Artificial generation of breaks in chromosome 1 by CRISPR-Cas9-mediated genome editing. Design and construction of genome-editing vectors for delivery of CRISPR-Cas9 components was performed following general protocols available from the Zheng lab (16) and as previously described (3). Six different 20-nucleotide guide RNA (gRNA) sequences were designed to target the region on chromosome 1q42 defined by LMPCR to contain the HCMV-induced break sites. The following are the targeted 1q42 sequences:

1q42-1: 5′-CTCTTTCTAGAAGCCGTTAG-3′
1q42-2: 5′-AAGATTCGTCCTGTAGCACG-3′
1q42-3: 5′-ACGACTGCTCGCCTACATGT-3′
1q42-4: 5′-TTCTCATCGAGCAGTGTATT-3′
1q42-5: 5′-GCTCACTCAACATCCGCCTA-3′
1q42-6: 5′-ATACGAAAATTAGCCGGGCG-3′

Guide RNAs were inserted into the lentiCRISPRv2.0 (v2.0) vector (Addgene, 52961). The vector backbone was used as a negative control for targeting and selection. Lentivirus production, transduction, and selection to create pooled populations of THF cells were as described above.

After puromycin selection, the efficiency of genome editing of the pools was verified using the comparison algorithm tracking of indels by decomposition (TIDE) developed by Brinkman and colleagues (17) (https://tide.nki.nl/). Briefly, genomic DNA was isolated from cells of CRISPR pools 1q42-1 to 1q42-6. An approximately 1-kb region encompassing all the targets was amplified using the forward primer 1q42-1N1 (see Table 1 for sequence) and reverse primer 1q42-3R (5′-CAGTGTCCATCCATCAGTAAGAC-3′). Amplicons were then sequenced using either one of these two primers or an additional internal primer ($1q423F_{int}$: 5′-AGCTGGCTAAAAGGGAGGT-3′), with the ideal sequencing primer situated 200 to 400 bp from the position of the target site. Sequences from the CRISPR-targeted cells were then compared to those generated from the control-targeted cell pool (v2.0), and a percentage of targeting was determined using the TIDE software.

Immunofluorescence staining. Unless specified otherwise, cells on coverslips were harvested and fixed in 3% formaldehyde in 1× PBS containing 2.5% sucrose, followed by permeabilization in 1% Triton in 1× PBS containing 2.5% sucrose and 0.25 M glycine. Detection of CTCF and pp71 for confocal analysis of cells on coverslips was performed using an "extraction first" methodology as previously described (44). Immunofluorescence staining was performed as previously described (91). Glycerol mounting medium with 4′,6-diamidino-2-phylindole (DAPI) and DABCO (Electron Microscopy Science, 17989-60) was used to mount the coverslips (and simultaneously counterstain nuclei). Epifluorescence analysis was performed on a Nikon Eclipse E800 fluorescence microscope equipped with a Nikon DS-Ri1 high-resolution color camera and Nikon NIS Elements imaging software. Confocal analysis was performed using a Nikon/Andor spinning disk confocal microscope with NIS Elements acquisition software. Samples were excited using lasers at 488 nm for Alexa Fluor 488, 559 nm for tetramethyl rhodamine isothiocyanate (TRITC), and 405 nm for Hoechst. Confocal images were analyzed using Imaris software version 8.1.1 or

TABLE 2 ChIP primers used in this study

Sequence	Name
5′-TGAGCACTAGATGTCGGTAAAC-3′	CTCF F
5′-ACAGCTGCAAATCCCATATAGT-3′	CTCF R
5′-TCCTCTGATTAGGGTTGGGT-3′	NID1CTCF1_1F
5′-TACCAGGGTCAAGCGAATTG-3′	NID1CTCF1_1R
5′-CTGCTCGAGGCCAACAT-3′	NID1CTCF1_2F
5′-GGGCGTCCGGTTACATC-3′	NID1CTCF1_2R

8.2.0. Primary Abs used were mouse monoclonal Abs anti-IE1 (clone p63-27 [IgG2A]; a gift from B. Britt, University of Alabama, Birmingham) and anti-pp71 (clone IE233 [IgG1]; a gift from R. Kalejta, University of Wisconsin, Madison) and rabbit anti-CTCF (Bethyl, A300-543A). Secondary Abs used were goat anti-mouse IgG2A coupled with Alexa Fluor 488 (Molecular Probes, A-21131), goat anti-mouse IgG1 coupled with TRITC (Southern Biotech, 1070-03), goat anti-mouse IgG1 coupled with Alexa Fluor 488 (Molecular Probes, A-21121), and donkey anti-rabbit coupled with TRITC (Jackson Immunoresearch, 711-025-152).

Western blotting analysis. Cells were harvested, counted, and stored as pellets at −80°C until use. Cell lysates were prepared as previously described (47). Lysates from equivalent cells were run on 8% SDS-polyacrylamide gels (except blots to detect UL35/UL35A, which were 12%). After electrophoresis, proteins were transferred to a Protran membrane (GE Healthcare Life Sciences, 10600002). The membranes were incubated with specific Abs for protein detection and were developed using a WesternBright Quantum kit (Advansta, K-12042-D20) as previously described (44). Lamin B or pan-actin were used as loading controls for protein analyses. Primary Abs used included mouse anti-NID1 (clone 302117; R&D Systems, MAB2570-100), mouse anti-IE1 and IE2 (clone CH16.0; Virusys, P1215), mouse anti-IE1 (clone p63-27), mouse anti-pp65 (clone CH12; Virusys, P1205), mouse anti-pp71 (clone IE233), mouse anti-pan-actin (clone Ab-5; NeoMarkers, MS-1295-P), mouse anti-HA tag (clone 12CA5; Abgent, AM1008A), rabbit anti-UL35 and UL35A (clone BIE-1; a gift from B. Biegalke [24]), rabbit anti-CTCF, and rabbit anti-lamin B1 (Proteintech, 12987-1-AP). Secondary Abs used were sheep anti-mouse IgG (Jackson Immunoresearch, 515-035-062) and donkey anti-rabbit IgG (GE Healthcare, NA934V), both conjugated with horseradish peroxidase.

(i) Western blot quantitation. For each sample to be quantitated, Quantity One software was used to first subtract surrounding background pixel density and then measure pixel density for NID1 and the loading control. A normalized value for the NID1 density was obtained by dividing NID1 density by loading control density. These normalized values could then be compared, virus/mock (V/M), to obtain the appropriate ratio. Fold changes for treated versus untreated samples were obtained by dividing the V/M ratio of treated samples by the V/M ratio of untreated samples. For CRISPR-treated cells (Fig. 1D or Fig. S1B), normalized values were compared, CRISPR-treated/v2.0-treated, to obtain the appropriate ratios.

Real-time quantitative PCR (RT-qPCR) assay. Cells were harvested and stored as pellets at −80°C until use. RNA was extracted using an SV total RNA isolation system kit (Promegan, Z3100), and cDNA was synthesized as previously described (3). RT-qPCR assays were performed as described previously (3) with minor modifications. In brief, quantification was conducted using a StepOnePlus real-time PCR system (Applied Biosystems). Freshly synthesized cDNAs were diluted at 1:100 just before the RT-qPCR assay. Each reaction was performed in a 20-μL volume that contained 8 μL of diluted cDNA and 10 μL of PowerUp SYBR green master mix (Applied Biosystems), with a final concentration of 0.4 μM of each primer for *NID1*, *G6PD*, or *pp71*. Specific forward and reverse primers, respectively, were *NID1* (5′-GTG GATGCAGGCACCAATCGG-3′ and 5′-GGGCCGTGGTGATGCCATAC-3′), *G6PD* (5′-GAGGTGGGATGGGGTGC CCTTC-3′ and 5′-CGCTCGTAGGCGTCAGGGAGC-3′), and *pp71* (5′-CGTGGGTTTTGGACTCTCAC-3′ and 5′-C CTCTTCCTCTTCTTCCTCCTC-3′). All test samples were performed in triplicate for target genes and the endogenous control, *G6PD*. A no-template control (NTC) for each primer pair was included to monitor for contamination of the reagents in each assay. Each RT-qPCR was performed on a MicroAmp fast 96-well reaction plate (Applied Biosystems) with the following running conditions: 95°C for 10 min, 40 cycles of 95°C for 15 s, and 60°C for 1 min for all genes. To determine the presence of a single PCR product for each primer set, a melting curve was run at the end of each RT-qPCR assay from 60°C to 95°C.

Each primer set met an amplification efficiency between 93 and 105%, with a coefficient of determination (R^2) of ≥0.99. To calculate the relative gene expression, the threshold cycle (C_T) values for each gene in each sample were averaged across the technical triplicates, and the target gene expression was normalized to *G6PD*. The log fold change and the relative gene expression were presented according to the $2^{-\Delta\Delta CT}$ method (92). In each panel representing transcript data, the mock- or Adic-infected cells were used as the reference sample. Therefore, a sample with a decreased level of transcripts would appear as a negative number. Data shown are one representative experiment from at least two independent experiments.

Chromatin immunoprecipitation (ChIP) qPCR assay. ChIP assays were performed according to the Upstate Biotechnology, Inc., protocol, as described previously, with minor modifications (64). Briefly, cells were fixed in 1% formaldehyde for 15 min, and DNA was sonicated using a Fisher Model 500 cuphorn sonicator to generate 200- to 500-bp fragments. Chromatin was immunoprecipitated with 4 μg of Abs specific for CTCF (Active Motif, 61311) or pp71 (a mix of mouse monoclonal Abs IE233 and 2H10-9; R. Kalejta). Real-time PCR was performed with a master mix containing 1× Maxima SYBR green, 0.25 μM primers, and 1/50 of the ChIP DNA per well. Quantitative PCR assays were performed in triplicate using the ABI StepOnePlus PCR system. Data were analyzed by the $\Delta\Delta C_T$ method relative to DNA input and

normalized to the mock- or Adic-infected control and expressed as fold enrichment over that control (V/M or Adpp71/Adic, respectively). Primers used are listed in Table 2.

Fig. 8B shows data utilizing the NID1CTCF1-1F and NID1CTCF1-1R primers. In Fig. 8C and D, the NID1CTCF1-2F and NID1CTCF1-2R primers were used.

Statistical analysis. All analyses were performed using GraphPad Prism 8 software. Paired *t* tests with two tails were used for all the Western blotting and cell count analyses (Fig. S2 in the supplemental material). For analysis of ChIP data, nonparametric, two-tailed *t* tests were used. Statistical significance between groups was as follows for all analyses: n.s., nonsignificant; n.s.$^{\Delta}$, *P* value between 0.05 and 0.08; *, $P < 0.05$; **, $P < 0.01$; ***, $P < 0.001$.

Data availability. Underlying data are available upon request.

SUPPLEMENTAL MATERIAL

Supplemental material is available online only.

SUPPLEMENTAL FILE 1, PDF file, 0.8 MB.

ACKNOWLEDGMENTS

We thank Wade Bresnahan, Robert Kalejta, Bonita Biegalke, Lori Frappier, Peggy Wallace, William Britt, and Daniel Streblow for the gift of reagents for our studies; Rebecca Brown, Kayla Martin, Emmerentia Marx, and Alexandra Faeth for technical assistance; James Deringer for assistance in CRISPR construct design; and Emmanuel Ijezie for helpful discussions and comments on the manuscript.

We also acknowledge the following funding sources: NIH AI130209 to I.T., NIH AI051463 and AI139503 to E.A.F., NIH Idaho INBRE P20 RR016454 and Idaho WWAMI Medical program (bridging funds to E.A.F.), and NIH Idaho CMCI P20 GM104420 (imaging equipment usage). The funders had no role in study design, data collection and analysis, decision to publish, or preparation of the manuscript.

REFERENCES

1. Lee CH, Grey F. 2020. Systems virology and human cytomegalovirus: using high throughput approaches to identify novel host-virus interactions during lytic infection. Front Cell Infect Microbiol 10:280. https://doi.org/10.3389/fcimb.2020.00280.
2. Fortunato EA, Dell'Aquila ML, Spector DH. 2000. Specific chromosome 1 breaks induced by human cytomegalovirus. Proc Natl Acad Sci U S A 97:853–858. https://doi.org/10.1073/pnas.97.2.853.
3. Kuan MI, Jaeger HK, Balemba OB, O'Dowd JM, Duricka D, Hannemann H, Marx E, Teissier N, Gabrielli L, Bonasoni MP, Keithley EM, Fortunato EA. 2021. Human cytomegalovirus interactions with the basement membrane protein Nidogen 1. J Virol 95:e01506-20. https://doi.org/10.1128/JVI.01506-20.
4. Nightingale K, Lin KM, Ravenhill BJ, Davies C, Nobre L, Fielding CA, Ruckova E, Fletcher-Etherington A, Soday L, Nichols H, Sugrue D, Wang ECY, Moreno P, Umrania Y, Huttlin EL, Antrobus R, Davison AJ, Wilkinson GWG, Stanton RJ, Tomasec P, Weekes MP. 2018. High-definition analysis of host protein stability during human cytomegalovirus infection reveals antiviral factors and viral evasion mechanisms. Cell Host Microbe 24:447–460. https://doi.org/10.1016/j.chom.2018.07.011.
5. Tirosh O, Cohen Y, Shitrit A, Shani O, Le-Trilling VT, Trilling M, Friedlander G, Tanenbaum M, Stern-Ginossar N. 2015. The transcription and translation landscapes during human cytomegalovirus infection reveal novel host-pathogen interactions. PLoS Pathog 11:e1005288. https://doi.org/10.1371/journal.ppat.1005288.
6. Weekes MP, Tomasec P, Huttlin EL, Fielding CA, Nusinow D, Stanton RJ, Wang ECY, Aicheler R, Murrell I, Wilkinson GWG, Lehner PJ, Gygi SP. 2014. Quantitative temporal viromics: an approach to investigate host-pathogen interaction. Cell 157:1460–1472. https://doi.org/10.1016/j.cell.2014.04.028.
7. Tsuprun V, Santi P. 2001. Proteoglycan arrays in the cochlear basement membrane. Hear Res 157:65–76. https://doi.org/10.1016/s0378-5955(01)00278-7.
8. Dziadek M. 1995. Role of laminin-nidogen complexes in basement membrane formation during embryonic development. Experientia 51:901–913. https://doi.org/10.1007/BF01921740.
9. Miosge N, Holzhausen S, Zelent C, Sprysch P, Herken R. 2001. Nidogen-1 and nidogen-2 are found in basement membranes during human embryonic development. Histochem J 33:523–530. https://doi.org/10.1023/a:1014995523521.
10. Stiemer B, Springmeier G, el-Jarad L, Schroter-Kermani C. 1993. Matrix production of smooth muscle cells from rat aorta in vitro. Histol Histopathol 8:63–72.
11. Lee SH, Kalejta RF, Kerry J, Semmes OJ, O'Connor CM, Khan Z, Garcia BA, Shenk T, Murphy E. 2012. BclAF1 restriction factor is neutralized by proteasomal degradation and microRNA repression during human cytomegalovirus infection. Proc Natl Acad Sci U S A 109:9575–9580. https://doi.org/10.1073/pnas.1207496109.
12. Reinhardt B, Vaida B, Voisard R, Keller L, Breul J, Metzger H, Herter T, Baur R, Luske A, Mertens T. 2003. Human cytomegalovirus infection in human renal arteries in vitro. J Virol Methods 109:1–9. https://doi.org/10.1016/s0166-0934(03)00035-1.
13. Reinhardt B, Winkler M, Schaarschmidt P, Pretsch R, Zhou S, Vaida B, Schmid-Kotsas A, Michel D, Walther P, Bachem M, Mertens T. 2006. Human cytomegalovirus-induced reduction of extracellular matrix proteins in vascular smooth muscle cell cultures: a pathomechanism in vasculopathies? J Gen Virol 87:2849–2858. https://doi.org/10.1099/vir.0.81955-0.
14. Nobre LV, Nightingale K, Ravenhill BJ, Antrobus R, Soday L, Nichols J, Davies JA, Seirafian S, Wang EC, Davison AJ, Wilkinson GW, Stanton RJ, Huttlin EL, Weekes MP. 2019. Human cytomegalovirus interactome analysis identifies degradation hubs, domain associations and viral protein functions. eLife 8:e49894. https://doi.org/10.7554/eLife.49894.
15. Kong Q, Maizels N. 2001. Breaksite batch mapping, a rapid method for assay and identification of DNA breaksites in mammalian cells. Nucleic Acids Res 29:E33. https://doi.org/10.1093/nar/29.6.e33.
16. Cong L, Ran FA, Cox D, Lin S, Barretto R, Habib N, Hsu PD, Wu X, Jiang W, Marraffini LA, Zhang F. 2013. Multiplex genome engineering using CRISPR/Cas systems. Science 339:819–823. https://doi.org/10.1126/science.1231143.
17. Brinkman EK, Chen T, Amendola M, van Steensel B. 2014. Easy quantitative assessment of genome editing by sequence trace decomposition. Nucleic Acids Res 42:e168. https://doi.org/10.1093/nar/gku936.
18. Tang Q, Maul GG. 2006. Mouse cytomegalovirus crosses the species barrier with help from a few human cytomegalovirus proteins. J Virol 80:7510–7521. https://doi.org/10.1128/JVI.00684-06.
19. Ishov AM, Vladimirova OV, Maul GG. 2002. Daxx-mediated accumulation of human cytomegalovirus tegument protein pp71 at ND10 facilitates initiation of viral infection at these nuclear domains. J Virol 76:7705–7712. https://doi.org/10.1128/jvi.76.15.7705-7712.2002.

20. Marshall KR, Rowley KV, Rinaldi A, Nicholson IP, Ishov AM, Maul GG, Preston CM. 2002. Activity and intracellular localization of the human cytomegalovirus protein pp71. J Gen Virol 83:1601–1612. https://doi.org/10.1099/0022-1317-83-7-1601.
21. Hensel GM, Meyer HH, Buchmann I, Pommerehne D, Schmolke S, Plachter B, Radsak K, Kern HF. 1996. Intracellular localization and expression of the human cytomegalovirus matrix phosphoprotein pp71 (ppUL82): evidence for its translocation into the nucleus. J Gen Virol 77:3087–3097. https://doi.org/10.1099/0022-1317-77-12-3087.
22. Kalejta RF. 2008. Tegument proteins of human cytomegalovirus. Microbiol Mol Biol Rev 72:249–265. https://doi.org/10.1128/MMBR.00040-07.
23. Salsman J, Wang X, Frappier L. 2011. Nuclear body formation and PML body remodeling by the human cytomegalovirus protein UL35. Virology 414:119–129. https://doi.org/10.1016/j.virol.2011.03.013.
24. Liu Y, Biegalke BJ. 2002. The human cytomegalovirus UL35 gene encodes two proteins with different functions. J Virol 76:2460–2468. https://doi.org/10.1128/jvi.76.5.2460-2468.2002.
25. Salsman J, Jagannathan M, Paladino P, Chan PK, Dellaire G, Raught B, Frappier L. 2012. Proteomic profiling of the human cytomegalovirus UL35 gene products reveals a role for UL35 in the DNA repair response. J Virol 86:806–820. https://doi.org/10.1128/JVI.05442-11.
26. Dwarakanath RS, Clark CL, McElroy AK, Spector DH. 2001. The use of recombinant baculoviruses for sustained expression of human cytomegalovirus immediate early proteins in fibroblasts. Virology 284:297–307. https://doi.org/10.1006/viro.2001.0924.
27. Murphy EA, Streblow DN, Nelson JA, Stinski MF. 2000. The human cytomegalovirus IE86 protein can block cell cycle progression after inducing transition into the S phase of permissive cells. J Virol 74:7108–7118. https://doi.org/10.1128/jvi.74.15.7108-7118.2000.
28. Bresnahan WA, Hultman GE, Shenk T. 2000. Replication of wild-type and mutant human cytomegalovirus in life-extended human diploid fibroblasts. J Virol 74:10816–10818. https://doi.org/10.1128/jvi.74.22.10816-10818.2000.
29. Fazio MJ, O'Leary J, Kahari VM, Chen YQ, Saitta B, Uitto J. 1991. Human nidogen gene: structural and functional characterization of the 5′-flanking region. J Invest Dermatol 97:281–285. https://doi.org/10.1111/1523-1747.ep12480380.
30. Bloom DC, Giordani NV, Kwiatkowski DL. 2010. Epigenetic regulation of latent HSV-1 gene expression. Biochim Biophys Acta 1799:246–256. https://doi.org/10.1016/j.bbagrm.2009.12.001.
31. Chen H-S, Martin KA, Lu F, Lupey LN, Mueller JM, Lieberman PM, Tempera I. 2014. Epigenetic deregulation of the LMP1/LMP2 locus of Epstein-Barr virus by mutation of a single CTCF-cohesin binding site. J Virol 88:1703–1713. https://doi.org/10.1128/JVI.02209-13.
32. Amelio AL, McAnany PK, Bloom DC. 2006. A chromatin insulator-like element in the herpes simplex virus type 1 latency-associated transcript region binds CCCTC-binding factor and displays enhancer-blocking and silencing activities. J Virol 80:2358–2368. https://doi.org/10.1128/JVI.80.5.2358-2368.2006.
33. Ertel MK, Cammarata AL, Hron RJ, Neumann DM. 2012. CTCF occupation of the herpes simplex virus 1 genome is disrupted at early times postreactivation in a transcription-dependent manner. J Virol 86:12741–12759. https://doi.org/10.1128/JVI.01655-12.
34. Tempera I, Lieberman PM. 2014. Epigenetic regulation of EBV persistence and oncogenesis. Semin Cancer Biol 26:22–29. https://doi.org/10.1016/j.semcancer.2014.01.003.
35. Tempera I, Klichinsky M, Lieberman PM. 2011. EBV latency types adopt alternative chromatin conformations. PLoS Pathog 7:e1002180. https://doi.org/10.1371/journal.ppat.1002180.
36. Tempera I, Wiedmer A, Dheekollu J, Lieberman PM. 2010. CTCF prevents the epigenetic drift of EBV latency promoter Qp. PLoS Pathog 6:e1001048. https://doi.org/10.1371/journal.ppat.1001048.
37. Chau CM, Zhang X-Y, McMahon SB, Lieberman PM. 2006. Regulation of Epstein-Barr virus latency type by the chromatin boundary factor CTCF. J Virol 80:5723–5732. https://doi.org/10.1128/JVI.00025-06.
38. Lee JS, Raja P, Pan D, Pesola JM, Coen DM, Knipe DM. 2018. CCCTC-binding factor acts as a heterochromatin barrier on herpes simplex viral latent chromatin and contributes to poised latent infection. mBio 9:e02372-17. https://doi.org/10.1128/mBio.02372-17.
39. Washington SD, Musarrat F, Ertel MK, Backes GL, Neumann DM. 2018. CTCF binding sites in the herpes simplex virus 1 genome display site-specific CTCF occupation, protein recruitment, and insulator function. J Virol 92:e00156-18. https://doi.org/10.1128/JVI.00156-18.
40. Washington SD, Singh P, Johns RN, Edwards TG, Mariani M, Frietze S, Bloom DC, Neumann DM. 2019. The CCCTC binding factor, CTRL2, modulates heterochromatin deposition and the establishment of herpes simplex virus 1 latency *in vivo*. J Virol 93:e00415-19. https://doi.org/10.1128/JVI.00415-19.
41. Elder EG, Krishna BA, Poole E, Perera M, Sinclair J. 2021. Regulation of host and viral promoters during human cytomegalovirus latency via US28 and CTCF. J Gen Virol 102:001609. https://doi.org/10.1099/jgv.0.001609.
42. Martinez FP, Cruz R, Lu F, Plasschaert R, Deng Z, Rivera-Molina YA, Bartolomei MS, Lieberman PM, Tang Q. 2014. CTCF binding to the first intron of the major immediate early (MIE) gene of human cytomegalovirus (HCMV) negatively regulates MIE gene expression and HCMV replication. J Virol 88:7389–7401. https://doi.org/10.1128/JVI.00845-14.
43. Cardoso MC, Leonhardt H, Nadal-Ginard B. 1993. Reversal of terminal differentiation and control of DNA replication: cyclin A and Cdk2 specifically localize at subnuclear sites of DNA replication. Cell 74:979–992. https://doi.org/10.1016/0092-8674(93)90721-2.
44. Kuan MI, O'Dowd JM, Fortunato EA. 2016. The absence of p53 during human cytomegalovirus infection leads to decreased UL53 expression, disrupting UL50 localization to the inner nuclear membrane, and thereby inhibiting capsid nuclear egress. Virology 497:262–278. https://doi.org/10.1016/j.virol.2016.07.020.
45. Lombard DB, Guarente L. 2000. Nijmegen breakage syndrome disease protein and MRE11 at PML nuclear bodies and meiotic telomeres. Cancer Res 60:2331–2334.
46. Kulkarni AS, Fortunato EA. 2011. Stimulation of homology-directed repair at I-SceI-induced DNA breaks during the permissive life cycle of human cytomegalovirus. J Virol 85:6049–6054. https://doi.org/10.1128/JVI.02514-10.
47. Luo MH, Rosenke K, Czornak K, Fortunato EA. 2007. Human cytomegalovirus disrupts both ataxia telangiectasia mutated protein (ATM)- and ATM-Rad3-related kinase-mediated DNA damage responses during lytic infection. J Virol 81:1934–1950. https://doi.org/10.1128/JVI.01670-06.
48. O'Dowd JM, Zavala AG, Brown CJ, Mori T, Fortunato EA. 2012. HCMV-infected cells maintain efficient nucleotide excision repair of the viral genome while abrogating repair of the host genome. PLoS Pathog 8:e1003038. https://doi.org/10.1371/journal.ppat.1003038.
49. McDougall JK. 1971. Adenovirus-induced chromosome aberrations in human cells. J Gen Virol 12:43–51. https://doi.org/10.1099/0022-1317-12-1-43.
50. Stich HF, Vanhoosier GL, Trentin JJ. 1964. Viruses and mammalian chromosomes; chromosome aberrations by human adenovirus type 12. Exp Cell Res 34:400–403. https://doi.org/10.1016/0014-4827(64)90375-1.
51. zur Hausen H. 1967. Induction of specific chromosomal aberrations by adenovirus type 12 in human embryonic kidney cells. J Virol 1:1174–1185. https://doi.org/10.1128/JVI.1.6.1174-1185.1967.
52. Schramayr S, Caporossi D, Mak I, Jelinek T, Bacchetti S. 1990. Chromosomal damage induced by human adenovirus type 12 requires expression of the E1B 55-kilodalton viral protein. J Virol 64:2090–2095. https://doi.org/10.1128/JVI.64.5.2090-2095.1990.
53. Fortunato EA, Spector DH. 2003. Viral induction of site-specific chromosome damage. Rev Med Virol 13:21–37. https://doi.org/10.1002/rmv.368.
54. Yu A, Fan HY, Liao D, Bailey AD, Weiner AM. 2000. Activation of p53 or loss of the Cockayne syndrome group B repair protein causes metaphase fragility of human U1, U2, and 5S genes. Mol Cell 5:801–810. https://doi.org/10.1016/s1097-2765(00)80320-2.
55. Pavelitz T, Bailey AD, Elco CP, Weiner AM. 2008. Human U2 snRNA genes exhibit a persistently open transcriptional state and promoter disassembly at metaphase. Mol Cell Biol 28:3573–3588. https://doi.org/10.1128/MCB.00087-08.
56. Preston CM, Nicholl MJ. 2006. Role of the cellular protein hDaxx in human cytomegalovirus immediate-early gene expression. J Gen Virol 87:1113–1121. https://doi.org/10.1099/vir.0.81566-0.
57. Saffert RT, Kalejta RF. 2006. Inactivating a cellular intrinsic immune defense mediated by Daxx is the mechanism through which the human cytomegalovirus pp71 protein stimulates viral immediate-early gene expression. J Virol 80:3863–3871. https://doi.org/10.1128/JVI.80.8.3863-3871.2006.
58. Lukashchuk V, McFarlane S, Everett RD, Preston CM. 2008. Human cytomegalovirus protein pp71 displaces the chromatin-associated factor ATRX from nuclear domain 10 at early stages of infection. J Virol 82:12543–12554. https://doi.org/10.1128/JVI.01215-08.
59. Saffert RT, Kalejta RF. 2007. Human cytomegalovirus gene expression is silenced by Daxx-mediated intrinsic immune defense in model latent infections established in vitro. J Virol 81:9109–9120. https://doi.org/10.1128/JVI.00827-07.
60. Liu B, Stinski MF. 1992. Human cytomegalovirus contains a tegument protein that enhances transcription from promoters with upstream ATF and

AP-1 *cis*-acting elements. J Virol 66:4434–4444. https://doi.org/10.1128/JVI.66.7.4434-4444.1992.
61. Bresnahan WA, Shenk TE. 2000. UL82 virion protein activates expression of immediate early viral genes in human cytomegalovirus-infected cells. Proc Natl Acad Sci U S A 97:14506–14511. https://doi.org/10.1073/pnas.97.26.14506.
62. Lenarcic EM, Ziehr BJ, Moorman NJ. 2015. An unbiased proteomics approach to identify human cytomegalovirus RNA-associated proteins. Virology 481:13–23. https://doi.org/10.1016/j.virol.2015.02.008.
63. Tempera I, Deng Z, Atanasiu C, Chen C-J, D'Erme M, Lieberman PM. 2010. Regulation of Epstein-Barr virus OriP replication by poly(ADP-ribose) polymerase 1. J Virol 84:4988–4997. https://doi.org/10.1128/JVI.02333-09.
64. Lupey-Green LN, Caruso LB, Madzo J, Martin KA, Tan Y, Hulse M, Tempera I. 2018. PARP1 stabilizes CTCF binding and chromatin structure to maintain Epstein-Barr virus latency type. J Virol 92:e00755-18. https://doi.org/10.1128/JVI.00755-18.
65. Morgan SM, Tanizawa H, Caruso LB, Hulse M, Kossenkov A, Madzo J, Keith K, Tan Y, Boyle S, Lieberman PM, Tempera I. 2022. The three-dimensional structure of Epstein-Barr virus genome varies by latency type and is regulated by PARP1 enzymatic activity. Nat Commun 13:187. https://doi.org/10.1038/s41467-021-27894-1.
66. Fabits M, Goncalves Magalhaes V, Chan B, Girault V, Elbasani E, Rossetti E, Saeland E, Messerle M, Pichlmair A, Lisnic VJ, Brinkmann MM. 2020. The cytomegalovirus tegument protein UL35 antagonizes pattern recognition receptor-mediated type I IFN transcription. Microorganisms 8:790. https://doi.org/10.3390/microorganisms8060790.
67. Schierling K, Stamminger T, Mertens T, Winkler M. 2004. Human cytomegalovirus tegument proteins ppUL82 (pp71) and ppUL35 interact and cooperatively activate the major immediate-early enhancer. J Virol 78:9512–9523. https://doi.org/10.1128/JVI.78.17.9512-9523.2004.
68. Maschkowitz G, Gartner S, Hofmann-Winkler H, Fickenscher H, Winkler M. 2018. Interaction of human cytomegalovirus tegument proteins ppUL35 and ppUL35A with sorting nexin 5 regulates glycoprotein B (gpUL55) localization. J Virol 92:e00013-18. https://doi.org/10.1128/JVI.00013-18.
69. Adamson CS, Nevels MM. 2020. Bright and early: inhibiting human cytomegalovirus by targeting major immediate-early gene expression or protein function. Viruses 12:110. https://doi.org/10.3390/v12010110.
70. Kim Y-E, Lee J-H, Kim ET, Shin HJ, Gu SY, Seol HS, Ling PD, Lee CH, Ahn J-H. 2011. Human cytomegalovirus infection causes degradation of Sp100 proteins that suppress viral gene expression. J Virol 85:11928–11937. https://doi.org/10.1128/JVI.00758-11.
71. Liu X-J, Yang B, Huang S-N, Wu C-C, Li X-J, Cheng S, Jiang X, Hu F, Ming Y-Z, Nevels M, Britt WJ, Rayner S, Tang Q, Zeng W-B, Zhao F, Luo M-H. 2017. Human cytomegalovirus IE1 downregulates Hes1 in neural progenitor cells as a potential E3 ubiquitin ligase. PLoS Pathog 13:e1006542. https://doi.org/10.1371/journal.ppat.1006542.
72. Chau NH, Vanson CD, Kerry JA. 1999. Transcriptional regulation of the human cytomegalovirus US11 early gene. J Virol 73:863–870. https://doi.org/10.1128/JVI.73.2.863-870.1999.
73. Winkler M, Rice SA, Stamminger T. 1994. UL69 of human cytomegalovirus, an open reading frame with homology to ICP27 of herpes simplex virus, encodes a transactivator of gene expression. J Virol 68:3943–3954. https://doi.org/10.1128/JVI.68.6.3943-3954.1994.
74. Iskenderian AC, Huang L, Reilly A, Stenberg RM, Anders DG. 1996. Four of eleven loci required for transient complementation of human cytomegalovirus DNA replication cooperate to activate expression of replication genes. J Virol 70:383–392. https://doi.org/10.1128/JVI.70.1.383-392.1996.
75. Kerry JA, Priddy MA, Jervey TY, Kohler CP, Staley TL, Vanson CD, Jones TR, Iskenderian AC, Anders DG, Stenberg RM. 1996. Multiple regulatory events influence human cytomegalovirus DNA polymerase (UL54) expression during viral infection. J Virol 70:373–382. https://doi.org/10.1128/JVI.70.1.373-382.1996.
76. Rossetto CC, Tarrant-Elorza M, Pari GS. 2013. *Cis* and *trans* acting factors involved in human cytomegalovirus experimental and natural latent infection of CD14$^+$ monocytes and CD34$^+$ cells. PLoS Pathog 9:e1003366. https://doi.org/10.1371/journal.ppat.1003366.
77. Cheng S, Caviness K, Buehler J, Smithey M, Nikolich-Zugich J, Goodrum F. 2017. Transcriptome-wide characterization of human cytomegalovirus in natural infection and experimental latency. Proc Natl Acad Sci U S A 114:E10586–E10595. https://doi.org/10.1073/pnas.1710522114.
78. Shnayder M, Nachshon A, Krishna B, Poole E, Boshkov A, Binyamin A, Maza I, Sinclair J, Schwartz M, Stern-Ginossar N. 2018. Defining the transcriptional landscape during cytomegalovirus latency with single-cell RNA sequencing. mBio 9:e00013-18. https://doi.org/10.1128/mBio.00013-18.
79. Hu J, Yang Y, Turner PC, Jain V, McIntyre LM, Renne R. 2014. LANA binds to multiple active viral and cellular promoters and associates with the H3K4methyltransferase hSET1 complex. PLoS Pathog 10:e1004240. https://doi.org/10.1371/journal.ppat.1004240.
80. Tempera I, De Leo A, Kossenkov AV, Cesaroni M, Song H, Dawany N, Showe L, Lu F, Wikramasinghe P, Lieberman PM. 2016. Identification of MEF2B, EBF1, and IL6R as direct gene targets of Epstein-Barr virus (EBV) nuclear antigen 1 critical for EBV-infected B-lymphocyte survival. J Virol 90:345–355. https://doi.org/10.1128/JVI.02318-15.
81. DeFilippis VR, Alvarado D, Sali T, Rothenburg S, Fruh K. 2010. Human cytomegalovirus induces the interferon response via the DNA sensor ZBP1. J Virol 84:585–598. https://doi.org/10.1128/JVI.01748-09.
82. Li H, Chang L-J, Neubauer DR, Muir DF, Wallace MR. 2016. Immortalization of human normal and NF1 neurofibroma Schwann cells. Lab Invest 96:1105–1115. https://doi.org/10.1038/labinvest.2016.88.
83. Tamashiro JC, Hock LJ, Spector DH. 1982. Construction of a cloned library of the EcoRI fragments from the human cytomegalovirus genome (strain AD169). J Virol 42:547–557. https://doi.org/10.1128/JVI.42.2.547-557.1982.
84. Anglana M, Bacchetti S. 1999. Construction of a recombinant adenovirus for efficient delivery of the I-SceI yeast endonuclease to human cells and its application in the in vivo cleavage of chromosomes to expose new potential telomeres. Nucleic Acids Res 27:4276–4281. https://doi.org/10.1093/nar/27.21.4276.
85. Bett AJ, Haddara W, Prevec L, Graham FL. 1994. An efficient and flexible system for construction of adenovirus vectors with insertions or deletions in early regions 1 and 3. Proc Natl Acad Sci U S A 91:8802–8806. https://doi.org/10.1073/pnas.91.19.8802.
86. Kalejta RF, Bechtel JT, Shenk T. 2003. Human cytomegalovirus pp71 stimulates cell cycle progression by inducing the proteasome-dependent degradation of the retinoblastoma family of tumor suppressors. Mol Cell Biol 23:1885–1895. https://doi.org/10.1128/MCB.23.6.1885-1895.2003.
87. He TC, Zhou S, da Costa LT, Yu J, Kinzler KW, Vogelstein B. 1998. A simplified system for generating recombinant adenoviruses. Proc Natl Acad Sci U S A 95:2509–2514. https://doi.org/10.1073/pnas.95.5.2509.
88. Casavant NC, Luo MH, Rosenke K, Winegardner T, Zurawska A, Fortunato EA. 2006. Potential role for p53 in the permissive life cycle of human cytomegalovirus. J Virol 80:8390–8401. https://doi.org/10.1128/JVI.00505-06.
89. Kaspari M, Tavalai N, Stamminger T, Zimmermann A, Schilf R, Bogner E. 2008. Proteasome inhibitor MG132 blocks viral DNA replication and assembly of human cytomegalovirus. FEBS Lett 582:666–672. https://doi.org/10.1016/j.febslet.2008.01.040.
90. Ory DS, Neugeboren BA, Mulligan RC. 1996. A stable human-derived packaging cell line for production of high titer retrovirus/vesicular stomatitis virus G pseudotypes. Proc Natl Acad Sci U S A 93:11400–11406. https://doi.org/10.1073/pnas.93.21.11400.
91. Rosenke K, Samuel MA, McDowell ET, Toerne MA, Fortunato EA. 2006. An intact sequence-specific DNA-binding domain is required for human cytomegalovirus-mediated sequestration of p53 and may promote in vivo binding to the viral genome during infection. Virology 348:19–34. https://doi.org/10.1016/j.virol.2005.12.013.
92. Livak KJ, Schmittgen TD. 2001. Analysis of relative gene expression data using real-time quantitative PCR and the $2^{-\Delta\Delta}CT$ method. Methods 25:402–408. https://doi.org/10.1006/meth.2001.1262.